Dynamic analysis for the rotor drop process and its application to a vertically levitated rotor/AMB system

Yulan Zhao [1*], Guojun Yang [1], Patrick Keogh [2], Lei Zhao [1]

[1] Institute of Nuclear and New Energy Technology of Tsinghua University, Collaborative Innovation Center of Advanced Nuclear Energy Technology, the Key Laboratory of Advanced Reactor Engineering and Safety, Ministry of Education, Beijing, China, 100084

[2] Department of Mechanical Engineering, University of Bath, Bath, UK, BA2 7AY

Abstract

Active magnetic bearings (AMBs) have been utilized widely to support high-speed rotors. However, in the case of AMB failure, emergencies, or overload conditions, the auxiliary bearing is chosen as the backup protector to provide mechanical supports and displacement constraints for the rotor. With lack of support, the auxiliary bearing will catch the dropping rotor. Accordingly, high contact forces and corresponding thermal generation due to mechanical rub are applied on the dynamic contact area. Rapid deterioration may be brought about by excessive dynamic and thermal shocks. Therefore the auxiliary bearing must be sufficiently robust to guarantee the safety of the AMB system. Many approaches have been put forward in the literature to estimate the rotor dynamic motion, nonetheless most of them focus on the horizontal rotor drop and few consider the inclination around the horizontal plane for the vertical rotor. The main purpose of this paper is to predict the rotor dynamic behavior accurately for the vertical rotor drop case. A detailed model for the vertical rotor drop process with consideration of the rotating inclination around *x*- and *y*- axes is proposed in this paper. Additionally, rolling and sliding friction are distinguished in the simulation scenario. This model has been applied to estimate the rotor drop process in a helium circulator system equipped with AMBs for the 10 MW high-temperature gas-cooled reactor (HTR-10). The HTR-10 has been designed and researched by the Institute of Nuclear and New Energy Technology (INET) of Tsinghua University. The auxiliary bearing is utilized to support the rotor in the helium circulator. The validity of this model is verified by the results obtained in this paper as well. This paper also provides suggestions for the further improvement of auxiliary bearing design and engineering application.

Keywords: dynamic analysis; rotor drop; auxiliary bearing; active magnetic bearing; HTR-10

[*]Corresponding author

Tel.: +86 10 62797385 Fax: +86 10 62771150

E-mail address: zhaoyulan1989@163.com

1. Introduction

Active magnetic bearings (AMBs) have been recommended widely to support high-speed rotors in the industrial machinery field. They have advantages in terms of complete exemption of contact, wear contamination and lubrication, excellent endurance and well-controlled performance [1]. Additionally, an auxiliary bearing is usually assembled as the backup protector to provide mechanical support and displacement constraint for the rotor in cases of AMB failure, emergencies, or overload conditions. When an AMB is in normal operation, translational motions of the rotor in *x*-, *y*- and *z*- axes, and rotational motions around *x*- and *y*- axes in the horizontal plane are all controlled by the AMB system. The axial rotational motion of the rotor around *z*- axis is often governed by a motor. When the rotor drops down under gravity or due to overload, the auxiliary bearing will support the rotor within a smaller clearance than that of the AMB. The radial clearance of the auxiliary bearing is typically half the magnetic gap [2]. During the drop process the high-speed rotating rotor will make axial contact with the auxiliary bearing. Accordingly, high level thermal generation due to mechanical rub over the transient dynamic contact area is involved. Rapid deterioration may be brought about by excessive dynamic and thermal shocks. Therefore the auxiliary bearing must endure high mechanical and thermal shocks to mitigate rapid deterioration and to guarantee the integrity of the AMB system. Proposals to improve the reliability and stability of auxiliary bearings have been put forward though design and application. The complicated interaction in the rotor drop process must be understood. Simulation of the dynamic rotor drop process is a prerequisite for the upgrade of the auxiliary bearing design.

Many remarkable achievements have been accomplished in the literature to estimate the highly nonlinear dynamic process. In [3] the effects of auxiliary bearing parameters on system vibration were investigated with respect to friction, unbalance, stiffness and damping. Palazzolo et al. [4-6] considered rotor drop simulation of a flywheel energy storage system, numerically and experimentally. The effects of friction coefficient, support damping, and side load to reduce backward whirl were discussed in [4]. In addition, thermal growth of the rotor drop process was estimated in [5], and the fatigue life of auxiliary bearing in [6]. The results suggested therefore that the life of the auxiliary bearing can be extended by reducing auxiliary bearing clearance, dropping velocity, contact friction and support stiffness, applying static side-loads and increasing support. Keogh and Yong [7] indicated that the rotor drop procedure can be treated as a combination of bounce and rub. They simulated transient thermal response for a series of contact conditions. Moreover, an active recovery strategy was also obtained to make the rotor return from a persistent contact state back to a contact-free state [8]. The majority of reported researches involves horizontal rotor drop. However, in vertical rotor drop tests forward whirl is prevalent. Caprio et al. [9] provided a description of the design of a vertically oriented flywheel rotor/housing system and the rotor on the auxiliary bearing was demonstrated experimentally. A backup bearing system to the AMB, which was as part of the energy storage flywheel module, was developed and tested by Hawkins et al. [10, 11].

A full circle forward whirl was visible consistently in all tests. This whirl frequency does not change with speed for speeds above 2400 rpm, regardless of spin speed [10]. Furthermore in [11] serial tests were performed based on different magnetic bearing failure/fault cases. Ransom et al. [12] conducted a series of experiments and concluded that the rotor always shows a forward cylindrical subsynchronous whirl, which is not affected by the unbalance level or drop speed. To reveal the detailed interactions in the vertical rotor drop process, a systematic approach was presented by Wilkes et al. [13]. It is suggested that axial friction force can induce synchronous forward whirl when the rotational speed is below the natural frequency, and constant frequency whip when the rotational speed is above a whip frequency.

The 10 MW high-temperature gas-cooled reactor (HTR-10), renowned as the first modular high-temperature gas-cooled test reactor, has been designed and researched by the Institute of Nuclear and New Energy Technology (INET) of Tsinghua University in China [14]. The circulator is utilized to drive helium in the primary loop for energy exchange. In the helium circulator system of HTR-10, the rotor is levitated by radial and axial AMBs with auxiliary bearings assembled on the stator in this system [2]. Many studies on the auxiliary bearing have been carried out by the INET. Zhao et al. [15] studied dynamic responses and the strain field of the auxiliary bearing. The ability of the auxiliary bearing to resist axial and radial impacts in its loading limit was verified by Xiao et al. [16]. Results have shown that severe internal plastic deformation and damage to the auxiliary bearing performance are avoided. A dynamic model with consideration of axial and radial friction forces is established by Kang [17]. The influences of rotational frequency, stiffness and damping on the rotor dynamic behavior are evaluated accordingly. Furthermore Zhao et al. [18] estimated the thermal responses of this system by a detailed thermal model.

Many approaches have been put forward in the literature to estimate the rotor dynamic motion, nonetheless the vast majority of existing studies mainly focus on the horizontal rotor drop model and seldom consider the inclination around *x*- and *y*- axes in the horizontal plane. The main purpose of this paper is to predict the rotor dynamic behavior accurately for the vertical rotor drop. The axial contact between the rotor flange and the inner race of the auxiliary bearing adds to the level of the simulation complexity. Rolling and sliding friction are also included in the simulation. Thus the model is more accurate than that presented in the previous study [17]. This new model adds new features and precision. Furthermore, it is now possible to provide some suggestions for improvements to auxiliary bearing design and engineering application.

2. Dynamic rotor drop model

The detailed structure of the vertical model is shown in Fig.1. Two pairs of angular contact ball bearings are distributed at each end of the rotor. The upper auxiliary bearing endures the whole axial contact and part of the radial contact, and the lower one only endures part of the radial contact [2]. Rotor drop must relate to the interactions between the rotor and the auxiliary bearings. In vertical rotor drop

model the axial impact will firstly happen on the axial contact surface between the rotor flange and the inner race of the upper auxiliary bearing. High level mechanical rub will then ensue. Radial impact will subsequently occur due to normal contact forces and axial friction. The dynamic procedure is a combination of several contacts and bounces [7].

Given that three translational and two rotational motions lack support when AMB control is lost in the process of free rotor drop, they need to be simulated to describe the rotor dynamic motion. It is assumed that the rotor experiences gravity and interactions with the auxiliary bearing in the process of rotor drop. The rotational velocity is below any rotor bending critical modal frequency. The first-order critical frequency of the rotor is 160 Hz, which is much higher than the operating frequency of 83.3 Hz. Thus it is justifiable to treat the rotor as a rigid body as a first approximation. The analysis in this paper deals mainly with the following two aspects to reveal the rotor drop process: the axial and radial interactions and the detailed rotor dynamic model.

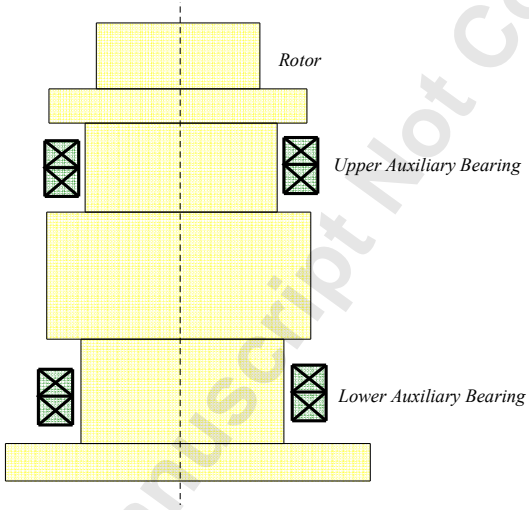

Fig 1. Rotor/auxiliary bearing system layout

2.1 Axial interaction between the rotor and the auxiliary bearings

Axial and radial interactions between the rotor and the auxiliary bearings have been assessed in preliminary studies [13]. The schematic of the rotor motion which involves translational and rotational motions is described in Fig.2. Here *x*, *y* and *z* are the translational displacements, and $\dot{\varphi}$ and $\dot{\theta}$ are the precession angular velocities of the rotor around *x*- and *y*- axes, respectively. In addition, z' denotes the rotating axis and $\dot{\gamma}$ the rotating velocity of the rotor. *a* and *b* denote the locations of the upper and lower auxiliary bearings with respect to the origin of the *xyz* system.

Journal of Tribology. Received April 21, 2016;
Accepted manuscript posted December 1, 2016. doi:10.1115/1.4035343

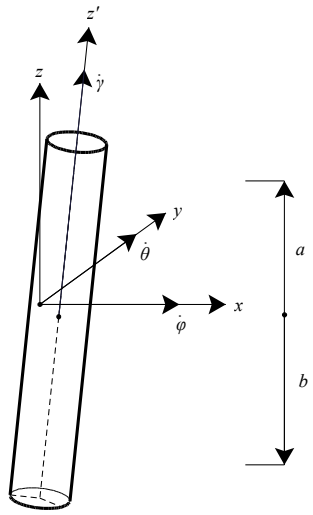

Fig 2. Rotor motion in fixed and rotating coordinates

Dynamic interactions are shown in Fig.3. Parameters α, ρ, and γ are chosen to describe the dynamic behavior of the rotor. O_b denotes the auxiliary bearing geometric center, O_r denotes the rotor geometric center and O_c denotes the rotor mass center, and α is the angle between O_bO_r and the x-axis. The whirling velocity of the rotor is $\dot{\alpha}$, while ρ denotes the relative distance between O_b and O_r, and γ is the rotational angle of the rotor.

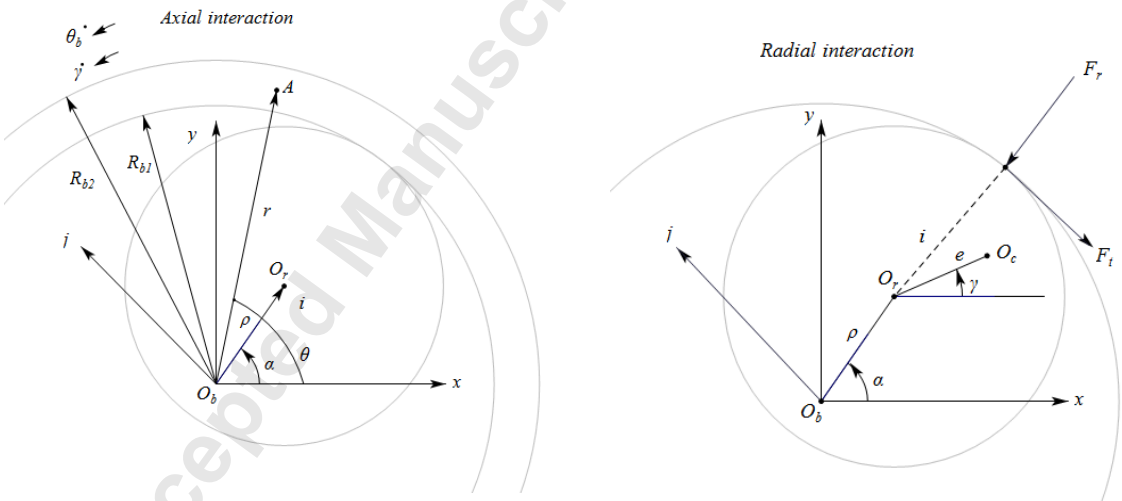

Fig 3. Dynamic interactions

Relative rotor to auxiliary bearing displacement is estimated to indicate whether contact happens. Axial contact happens when the axial penetration depth is positive. Similarly radial contact happens when the radial penetration depth is positive. The relationship of load and deflection during the rotor drop process can be obtained from a Hertz contact model. Thus the axial contact force generated by axial contact between the rotor and the upper auxiliary bearing can be represented as:

$$F_a = \begin{cases} K_a \delta_a^e + C_a \dot{\delta}_a, \delta_a > 0 \\ 0, \delta_a \le 0 \end{cases} \tag{1}$$

in which K_a denotes axial stiffness, C_a denotes axial contact damping, δ_a denotes axial impact depth and e denotes contact parameter applied to treat different contact conditions. Surface contact (e=1) happens on the axial contact surface between the rotor flange and the inner race of the auxiliary bearing, line contact (e=10/9) happens on the radial contact surface while point contact (e=3/2) occurs inside the auxiliary bearing [18].

The friction forces projected in i and j directions ($F_{af,i}$, $F_{af,j}$) and friction torque (T_a) applied on the axial contact surface in polar coordinate may be deduced from the preliminary study [18]:

$$F_{af,i} = -P_a \mu_a \int_{R_{b1}}^{R_{b2}} \int_0^{2\pi} \frac{\left[\dot{\rho} + \left(\dot{\gamma} - \dot{\theta}_b\right) r \sin\theta\right] \vec{i}}{\sqrt{\left[\dot{\rho} + \left(\dot{\gamma} - \dot{\theta}_b\right) r \sin\theta\right]^2 + \left[\dot{\alpha}\rho - \left(\dot{\theta}_b - \dot{\gamma}\right) r \cos\theta - \rho\dot{\gamma}\right]^2}} r d\theta dr \tag{2}$$

$$F_{af,j} = -P_a \mu_a \int_{R_{b1}}^{R_{b2}} \int_0^{2\pi} \frac{\left[\dot{\alpha}\rho + \left(\dot{\gamma} - \dot{\theta}_b\right) r \cos\theta - \rho\dot{\gamma}\right] \vec{j}}{\sqrt{\left[\dot{\rho} + \left(\dot{\gamma} - \dot{\theta}_b\right) r \sin\theta\right]^2 + \left[\dot{\alpha}\rho - \left(\dot{\theta}_b - \dot{\gamma}\right) r \cos\theta - \rho\dot{\gamma}\right]^2}} r d\theta dr \tag{3}$$

$$T_a = \frac{2\mu_a F_a \left(R_{b2}^3 - R_{b1}^3\right)}{3\left(R_{b2}^2 - R_{b1}^2\right)} \tag{4}$$

in which P_a denotes the axial contact pressure, μ_a the axial friction coefficient, $\dot{\theta}_b$ the velocity of the auxiliary bearing, R_{b1} and R_{b2} the inner and outer radii of the inner races, respectively.

The rotor drop can be explained as a combination of the following three processes [17]: free drop under gravity; backward whirling tendency; and forward whirling motion, driven by unbalance. These equations can explain the reason of the forward whirl dominance due to unbalance. The rotor has a backward whirling tendency when same velocity is not achieved. Subsequently, when the rotor and the bearings rotate together ($\dot{\gamma} = \dot{\theta}_b$), if the whirling velocity of the rotor is less than the self-rotating angular velocity ($\dot{\alpha} < \dot{\gamma}$), the axial friction force in j direction has positive value ($F_{af,j} > 0$). That is to say, axial contact friction will induce the tangential friction force in the same self-rotating direction and therefore it will enhance the forward whirling frequency. On the contrary, if the whirling velocity of the rotor is larger than the self-rotating angular velocity ($\dot{\alpha} > \dot{\gamma}$), then the axial friction force in j direction is negative ($F_{af,j} < 0$), which means axial friction force will induce forward whirl. This analysis shows that the axial friction force determines the forward whirl and drives the rotor in the direction of rotation. The axial contact force applied on the contact surface, the friction coefficient and the self-rotating velocity of the rotor also aggravate forward whirling motion. Furthermore, decreasing the rotor velocity is the most direct method to reduce the forward whirl motion. In the following analysis, a primary emphasis is placed on the influences of the rotor velocity and the friction coefficient on the rotor dynamic behavior.

2.2 Radial interaction between the rotor and the auxiliary bearings

With regard to radial contact, in the process of drop the rotor rotates with a significant rotational

velocity before colliding with the inner race of the auxiliary bearing. The radial contact force is:

$$F_r = \begin{cases} K_r \delta_r^e + C_r \dot{\delta}_r, \delta_r > 0 \\ 0, \delta_r \le 0 \end{cases} \tag{5}$$

in which K_r denotes radial stiffness, C_r radial contact damping, and δ_r radial impact depth.

Rotational motions in the upper and lower bearings are driven by the axial friction torque and the radial friction forces. Furthermore, rotational motions of the rotor and the inner races of the upper and lower auxiliary bearings are given by:

$$\ddot{\gamma} = -\frac{(F_{t1} + F_{t2}) R_r + T_a}{I_p} \tag{6}$$

$$\ddot{\theta}_{b1} = \frac{F_{t1} R_{b1} + T_a - T_{b1}}{I_b} \tag{7}$$

$$\ddot{\theta}_{b2} = \frac{F_{t2} R_{b1} - T_{b2}}{I_b} \tag{8}$$

in which I_p and I_b are the polar moment of inertia of the rotor and the moment of inertia of the auxiliary bearing, respectively. F_{t1} and F_{t2} are the tangential friction forces of the upper and lower bearings generated by radial collision respectively. T_{b1} and T_{b2} are the torque inside the upper and lower auxiliary bearings, which can be calculated by the Palmgren's empirical equations [19]:

$$T_{b,j} = T_{0,j} + T_{l,j} \quad j = 1, 2 \tag{9}$$

where T_0 is generated from the lubricating friction drag (with no load) and is influenced by the lubricating liquid, the bearing type, and the rotating velocity:

$$\begin{aligned} T_0 &= 10^{-7} f_0 (\upsilon n)^{2/3} d_m^3 \quad \upsilon n \ge 2000 \\ T_0 &= 160 \times 10^{-7} f_0 d_m^3 \quad \upsilon n \le 2000 \end{aligned} \tag{10}$$

in which υ ,the kinematic viscosity, and f_0, the lubricating factor, both relate to the lubrication properties. T_l reflects the elastic hysteresis and the friction loss caused by the partial differential sliding and can be calculated as:

$$T_l = f_1 P_1 d_m \tag{11}$$

where f_1 depends on the bearing design and load. P_1 denotes the equivalent dynamic load, and d_m the equivalent diameter.

A method of assessing whether rolling resistance occurs has been proposed [4]. Therefore this rolling condition is applied to determine the tangential contact force in the following analysis. When rolling friction happens on the contact surface of the upper auxiliary bearing, Eq. (12) is applied and is solved with Eqs. (6) and (7), simultaneously. Thus F_{t1} is obtained as:

$$R_r \dot{\gamma} = R_{b1} \dot{\theta}_{b1} \tag{12}$$

$$F_{t1} = \frac{-F_{t2} \cdot R_r^2 / I_p - T_a \left(R_r / I_p + R_{b1} / I_b \right) + T_{b1} \cdot R_{b1} / I_b}{R_r^2 / I_p + R_{b1}^2 / I_b} \tag{13}$$

in which F_{t2} is calculated due to sliding friction, $F_{t2} = \mu_d F_{r2}$, μ_d being the dynamic friction coefficient. Similarly, when rolling friction happens on the contact surface of the lower auxiliary bearing, it follows from Eqs. (6) and (8) that:

$$R_r\dot{\gamma} = R_{b1}\dot{\theta}_{b2} \tag{14}$$

$$F_{t2} = \frac{-F_{t1}\cdot R_r^2/I_p - T_a\cdot R_r/I_p + T_{b2}\cdot R_{b1}/I_b}{R_r^2/I_p + R_{b1}^2/I_b} \tag{15}$$

in which F_{t1} is calculated due to sliding friction, $F_{t1} = \mu_d F_{r1}$. In this rotor dynamic system there is rolling resistance on the surfaces of the upper and lower bearings. Then, using Eqs. (6), (7) and (8):

$$R_r\dot{\gamma} = R_{b1}\dot{\theta}_{b1} = R_{b1}\dot{\theta}_{b2} \tag{16}$$

$$F_{t1} = \frac{-\frac{R_r^2}{R_{b1}\cdot I_p}(T_a + T_{b1} + T_{b2}) - \frac{R_{b1}}{I_b}(T_a - T_{b1}) + \frac{R_r}{I_p}T_a}{2R_r^2/I_p + R_{b1}^2/I_b} \tag{17}$$

$$F_{t2} = F_{t1} + \frac{T_a - T_{b1} + T_{b2}}{R_{b1}} \tag{18}$$

It's important to note that if $F_{tj} > \mu_s F_{rj}$ ($j = 1,2$), this condition corresponds with sliding friction ($F_{tj} = \mu_d F_{rj}$). Similarly, if $F_{tj} < \mu_s F_{rj}$, rolling friction exists. In these formulas μ_s is the rolling friction coefficient. Another relevant point is that rolling friction happens when both the tangential velocity of the rotor and of the inner race are equal numerically. Tangential force influences the rotor motion greatly. If it changes direction, numerical instability may result. A numerical solution to the problem is obtained by the application of a small boundary to treat the zero relative velocity situation. The presupposed boundary of the relative velocity is 10^{-8} mm/s [4].Rolling friction only exists within this presupposed boundary. If the relative velocity exceeds this boundary, sliding friction is imposed.

2.3 Detailed dynamic rotor drop model

Three translational and two rotational motions of the rotor, (x, y, z, φ, θ), are considered to lose support through lack of AMB control, while $\dot{\gamma}$, which is the axial velocity of the rotor, can be still driven by the motor during the rotor drop process (Fig.2). The geometrical relationship can be elaborated by:

$$\begin{cases} x = \rho\cos\alpha = \dfrac{bx_1 + ax_2}{a+b} \\ y = \rho\sin\alpha = \dfrac{by_1 + ay_2}{a+b} \\ \varphi = -\dfrac{y_1 - y_2}{a+b} \\ \theta = -\dfrac{x_1 - x_2}{a+b} \end{cases} \tag{19}$$

in which x_1, y_1, x_2, y_2 are the displacements in the x- and y- axes of the upper and lower bearing cross sections, respectively. The motion of the mass center is governed by:

$$\begin{cases} \dot{x}_c = \dot{\rho}\cos\alpha - \dot{\alpha}\rho\sin\alpha - e\dot{\gamma}\sin\gamma \\ \dot{y}_c = \dot{\rho}\sin\alpha + \dot{\alpha}\rho\cos\alpha + e\dot{\gamma}\cos\gamma \end{cases} \tag{20}$$

In order to analyze the rotor dynamic behavior, the Lagrangian equation of motion is established through T and V, the kinetic energy and gravitational potential energy of the rotor, respectively:

$$\frac{d}{dt}\left(\frac{\partial T}{\partial \dot{q}_i}\right) - \frac{\partial T}{\partial q_i} + \frac{\partial V}{\partial q_i} = Q_i \tag{21}$$

$$T = \frac{1}{2}m\left(\dot{x}_c^2 + \dot{y}_c^2 + \dot{z}_c^2\right) + \frac{1}{2}I_p\dot{\varphi}^2 + \frac{1}{2}I_p\dot{\theta}^2 + \frac{1}{2}J\dot{\gamma}^2$$
$$= \frac{1}{2}m\dot{\rho}^2 + \frac{1}{2}m\dot{\alpha}^2\rho^2 + \frac{1}{2}me^2\dot{\gamma}^2 + me\dot{\rho}\dot{\gamma}\sin(\alpha-\gamma) + me\dot{\alpha}\rho\dot{\gamma}\cos(\alpha-\gamma) + \frac{1}{2}m\dot{z}^2 + \frac{1}{2}I_p\dot{\varphi}^2 + \frac{1}{2}I_p\dot{\theta}^2 + \frac{1}{2}J\dot{\gamma}^2 \quad (22)$$

$$V = mgz \quad (23)$$

in which e is the eccentricity of the rotor , q_i is the generalized coordinator and Q_i is the generalized force. Therefore the dynamic equations to assess the rotor drop process are obtained in the following equations:

$$\ddot{\alpha} = \frac{1}{\rho}\left[-e\dot{\gamma}^2\sin(\alpha-\gamma) - 2\dot{\rho}\dot{\alpha} - \frac{F_t}{m} + \frac{F_{af,j}}{m} - e\ddot{\gamma}\cos(\alpha-\gamma)\right] \quad (24)$$

$$\ddot{\rho} = \rho\dot{\alpha}^2 + e\dot{\gamma}^2\cos(\alpha-\gamma) - \frac{F_r}{m} - \frac{F_{af,i}}{m} - e\ddot{\gamma}\sin(\alpha-\gamma) \quad (25)$$

$$\ddot{\varphi} = \frac{-aF_{y1} + bF_{y2}}{I_p} \quad (26)$$

$$\ddot{\theta} = \frac{aF_{x1} - bF_{x2}}{I_p} \quad (27)$$

$$\ddot{z} = \frac{F_a}{m} - g \quad (28)$$

in which F_{x1}, F_{y1}, F_{x2} and F_{y2} mean the contact forces in Cartesian coordinate applied on the upper and lower bearing respectively. Also, $\ddot{\alpha}$ describes the whirling motion of the rotor. $\ddot{\rho}$ elaborates the rotor orbit in the horizontal plane. The angular acceleration around x- and y- axes, $\ddot{\varphi}$ and $\ddot{\theta}$ are analyzed using Eqs. (26) and (27). The axial displacement of the rotor, z, can be calculated by Eq. (28). Furthermore the rotational motions of the rotor and the inner races of the upper and lower auxiliary bearings have been described in the analysis above, shown in Eqs. (6), (7) and (8).

3. Results and discussion

The model was applied to the helium circulator system with the AMBs of HTR-10. The rotor is about 1.5 m long and 450 kg of mass, rotating at 5000 rpm in a normal operating condition. The ceramic ($S_{i3}N_4$) angular contact ball bearing with dry lubrication is selected as the auxiliary bearing type and applied in pairs. Both the upper bearing and the lower bearing are arranged in face to face. Moreover detailed parameters are described in Table.1 [2].

Numerical simulations were carried out to assess the rotor dynamic behavior. The pre-set simulation period was 0.5 s with variable integration time steps to simulate the initial contact moment. The simulation cases are listed in Table.2. Cases I-1 to 4 are estimated to reveal the rotor responses due to initial condition and unbalance. Cases II-1 to 3 are simulated to examine the effect of the friction coefficient. The simulation responses of Cases III-1 and 2 are compared and characterized to show that the initial velocity is a critical factor for the dynamic behavior of the rotor. Case IV simulates the rotor drop process with an aerodynamic loading force, which is generated by the blades mounted under the rotor of the helium circulator. In this simulation scenario the axial aerodynamic loading force is approximately 2000 N.

Table 1. System parameters

Rotor mass with circulator	450 kg
Length of rotor	1518 mm
Balance quality grade	G 6.3
Eccentricity	0.01 mm
Rotor speed	5000 rpm
Rotor first-order bending critical frequency	160 Hz
Polar moment of inertia (rotor)	7.9 kg · m^2
Transverse moment of inertia (rotor)	78. kg · m^2
Axial gap between auxiliary bearing and rotor	0.52 mm
Radial gap between auxiliary bearing and rotor	0.18 mm

Table 2. Simulation cases

Case	Initial Velocity	Friction Coefficient		Loading Force	Eccentricity
	(rpm)	Dynamic	Static	(N)	(mm)
I-1	5000	0.1	0.2	0	0.01
I-2*	5000	0.1	0.2	0	0.01
I-3	5000	0.1	0.2	0	0.02
I-4	5000	0.1	0.2	0	0.03
II-1	5000	0.2	0.3	0	0.01
II-2	5000	0.3	0.4	0	0.01
II-3	5000	0.4	0.5	0	0.01
III-1	4000	0.1	0.2	0	0.01
III-2	3000	0.1	0.2	0	0.01
IV	5000	0.1	0.2	2000	0.01

* Cases I-1 and 2 have different initial conditions.

3.1 Rotor drop model validation

The rotor dynamic behavior can be analyzed by the study of Case I-1. The rotor spins with full velocity, which is 5000 rpm. Accordingly, an experiment was also conducted. To evaluate the actual state, the initial condition is assumed that the initial center positions of the upper and lower bearings are in different quadrants with an initial velocity disturbance. The axial displacement of the rotor and its velocity are shown in Figs.4 and 5. The axial orbit obtained by the experiment is shown in Fig.6. A similar trend between the predicted rotor orbit and the measured rotor orbit is observed. It is clear that the rotor goes mainly through several significant bounces and then the vibration tends to be steady during

the intermittent contact period. Sustained axial bouncing is observed experimentally long after the simulations predict bouncing to have stopped. The axial displacement transducer was mounted on the stator housing, hence it measures relative rotor to stator displacement. This is considered to be the cause of the residual motion for $t > 0.2$ s, involving stator induced vibration. Stator vibrations are not included in the system model.

The predicted upper and lower orbits are shown in Figs.7 and 8, respectively. The red circle in the figure signifies the initial clearance between the rotor and the auxiliary bearing. The high-speed forward whirl in the upper rotor orbit has been fully developed over time after free fall, while more bounces are detected in the lower rotor orbit. The experimental orbits are plotted in Figs.9 and 10, which support the predicted findings. While the experimental results have some extra loops during the drop that may be related to unbalance. The angles around *x*- and *y*- axes obtained from the simulation have a similar variation tendency and are shown as Figs.11 and 12.

Rotor velocity decreases as shown in Fig.13. The rotor speed reduction is caused by the friction torque. A constant motor torque is assumed and the rotor speed change is only 0.4 rad/s. A motor under speed control would eliminate this, but clearly the changes would be very small. In addition the velocities of the upper and lower bearings are shown in Fig.14. After about 0.25 s the rotor and the bearings reach the same velocity and rotate together due to the large inertia difference. While an important aspect is that the upper bearing has a faster velocity acceleration than the lower bearing, this is due mainly to the driving torque applied on the axial contact surface. Furthermore, the whirling velocity of the rotor is revealed in Fig.15. The whirling velocity fluctuates rather dramatically in the initial period and then fluctuates smoothly in a certain range below the initial velocity.

The axial contact force is obtained in Fig.16. The rotor endures high impact initially. After several bounces the contact force undergoes a progressive decline and finally stabilizes to support the weight of the rotor. The axial contact force is entirely applied on the upper auxiliary bearing, which plays a crucial role to support the rotor during the rotor drop process. It is generally considered that more emphasis needs to be made to assess whether replacement is required. The maximal contact force in the first collision is about 5×10^4 N, and the following contact force is less than the first contact force. The maximal force is within the allowable load tolerance. Hence the auxiliary bearing during the short period of rotor drop with medium velocity is guaranteed away from excessive load deterioration.

Moreover axial friction torque is also shown in Fig.17. It is the main torque that propels the whirl motion of the rotor. The axial friction force is the cause of the forward whirl observed in the predicted orbits. The forces applied on the upper and lower bearings are also plotted in Figs.18 to 21. They show a similar tendency with each other, fluctuating rather drastically and then stabilizing within a rather narrow range. The peak contact force of the upper bearing is slightly higher than that of the lower bearing.

The effect of the rotor unbalance is considered in the analysis of Cases I-2 to and 4. It is assumed

that the rotor drops from the initial position without any velocity disturbance. Compared with Case I-1, the upper and lower orbits of Case I-2 are similar and the rotor responses as cylindrical motion. The predicted rotor orbits are plotted in Fig.22. With the increase of the eccentricity, the rotor behavior becomes more disordered. The rotor experiences a transition from cylindrical bouncing motion to circular rub motion. The centrifugal force applied on the rotor is accelerated by the unbalance. In the realistic experiments the unbalance even can induce extra loops, shown in Figs. 9 and 10.

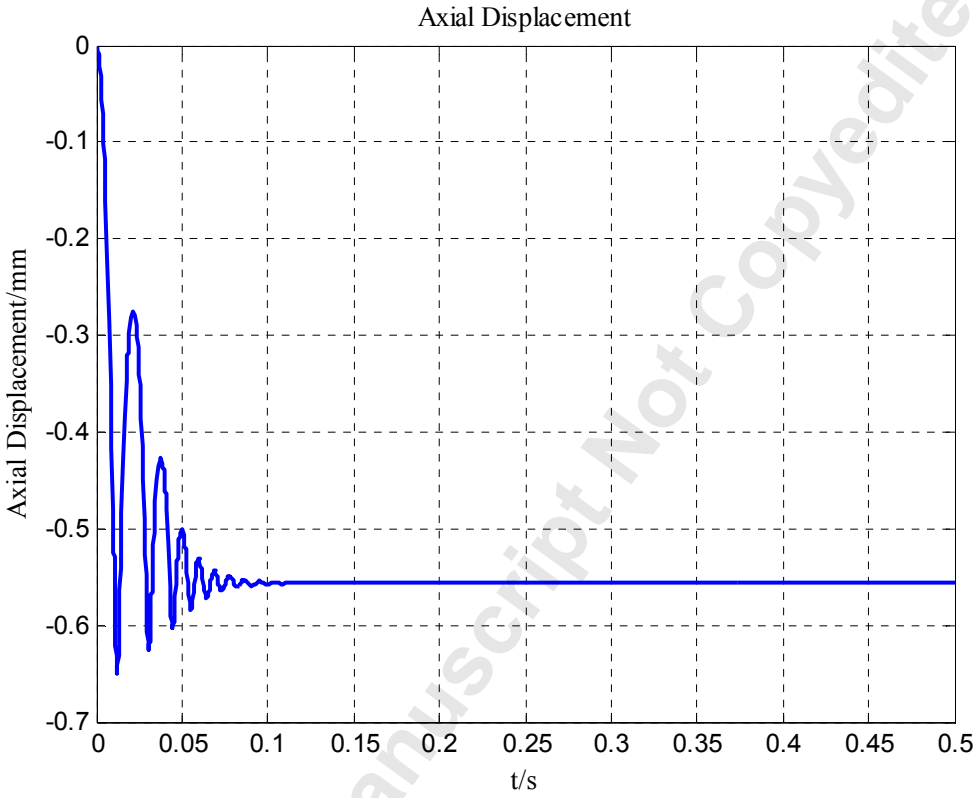

Fig 4. Predicted axial displacement, Case I-1

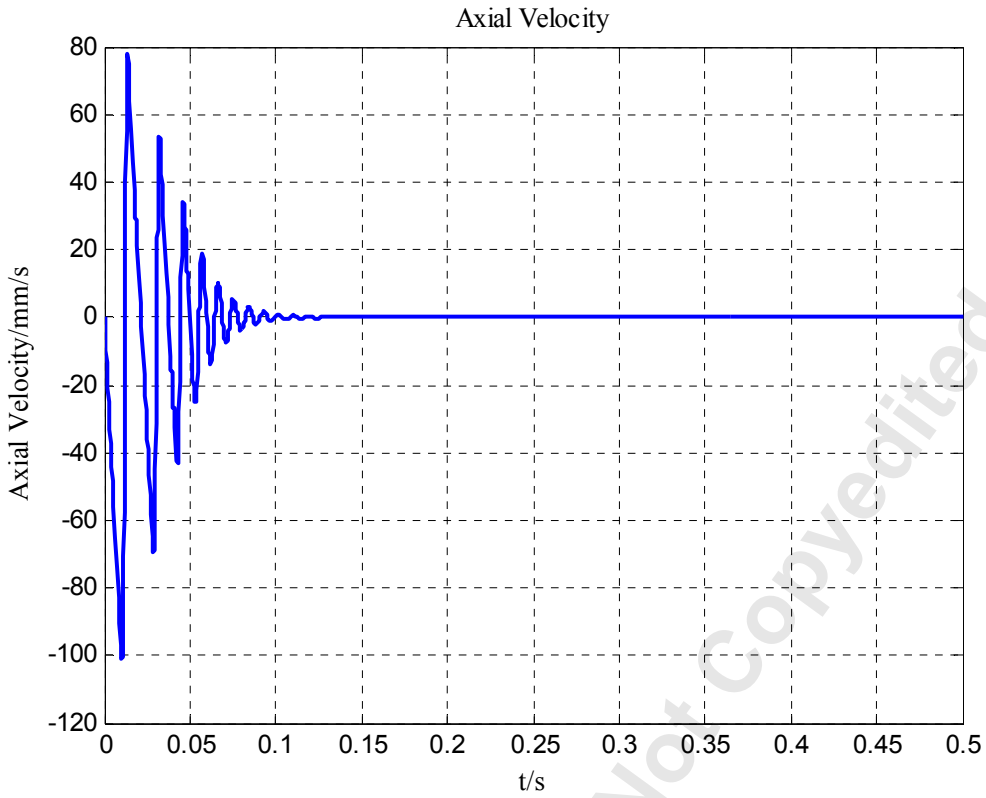

Fig 5. Axial velocity, Case I-1

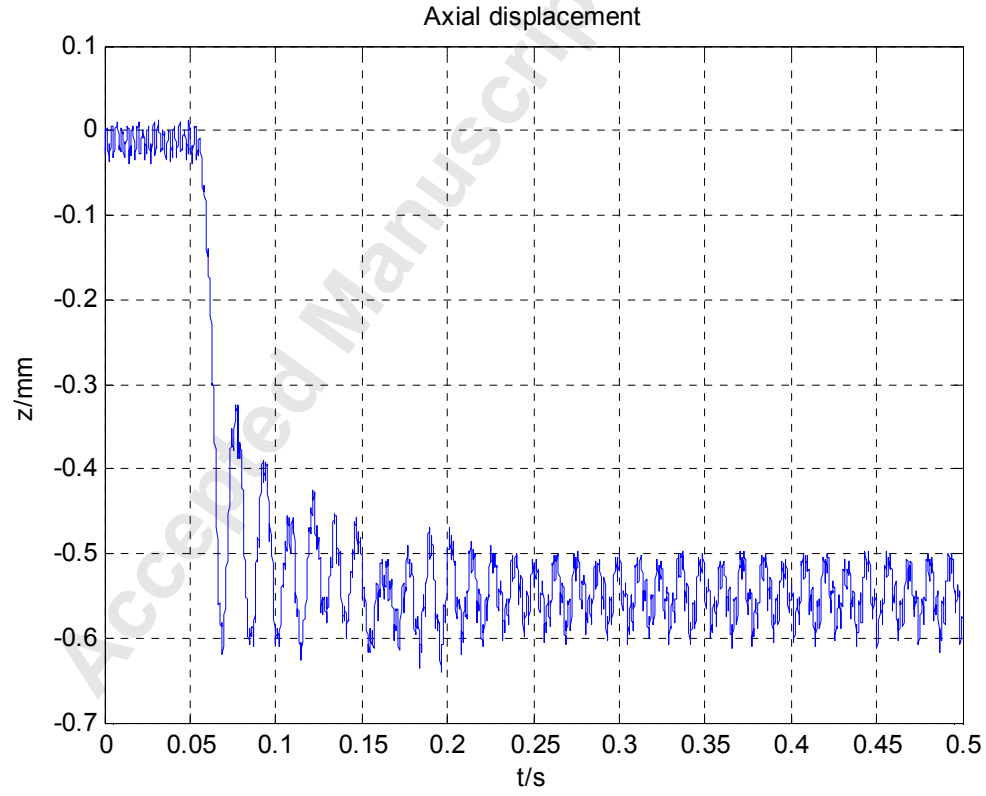

Fig 6. Experimental axial displacement, Case I-1

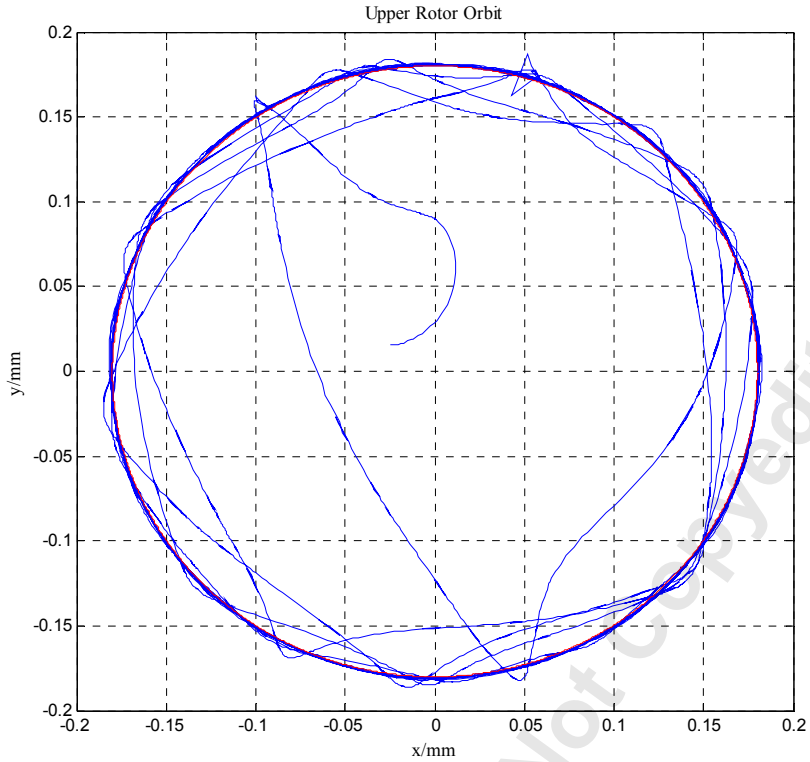

Fig 7. Predicted upper rotor orbit, Case I-1

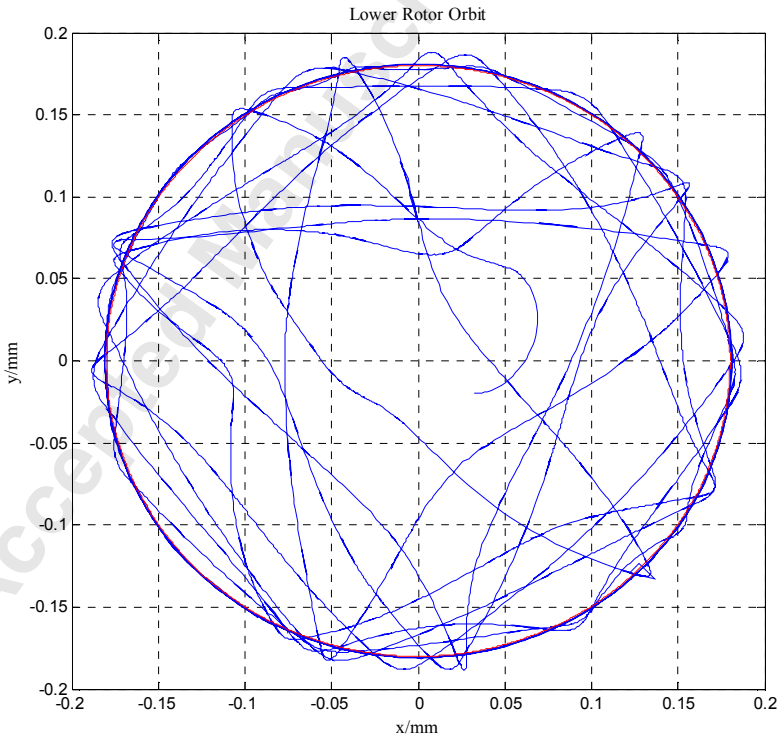

Fig 8. Predicted lower rotor orbit, Case I-1

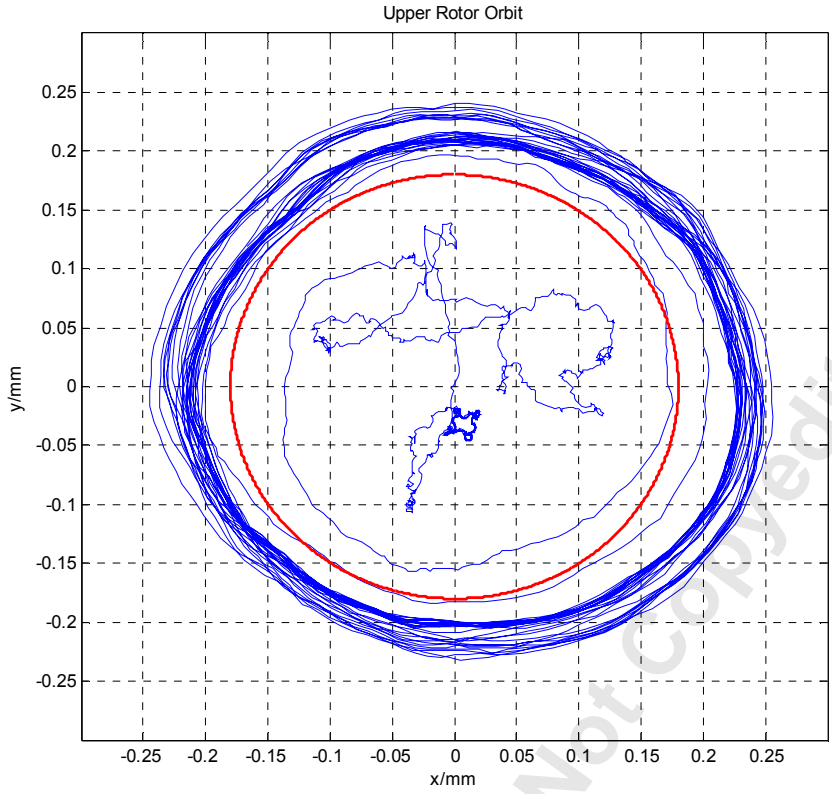

Fig 9. Experimental upper rotor orbit, Case I-1

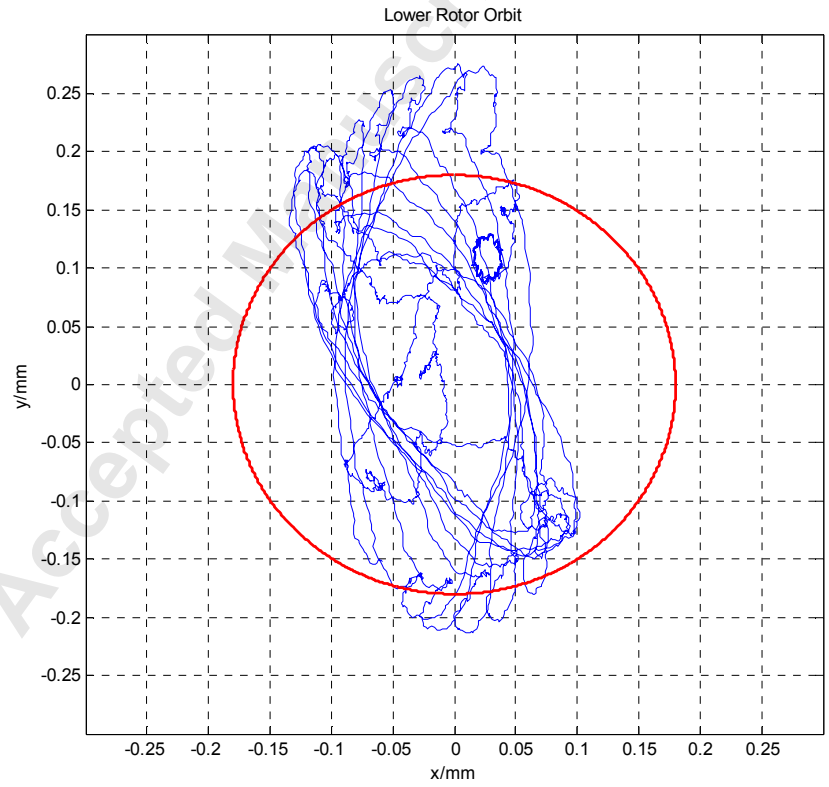

Fig 10. Experimental lower rotor orbit, Case I-1

Journal of Tribology. Received April 21, 2016;
Accepted manuscript posted December 1, 2016. doi:10.1115/1.4035343

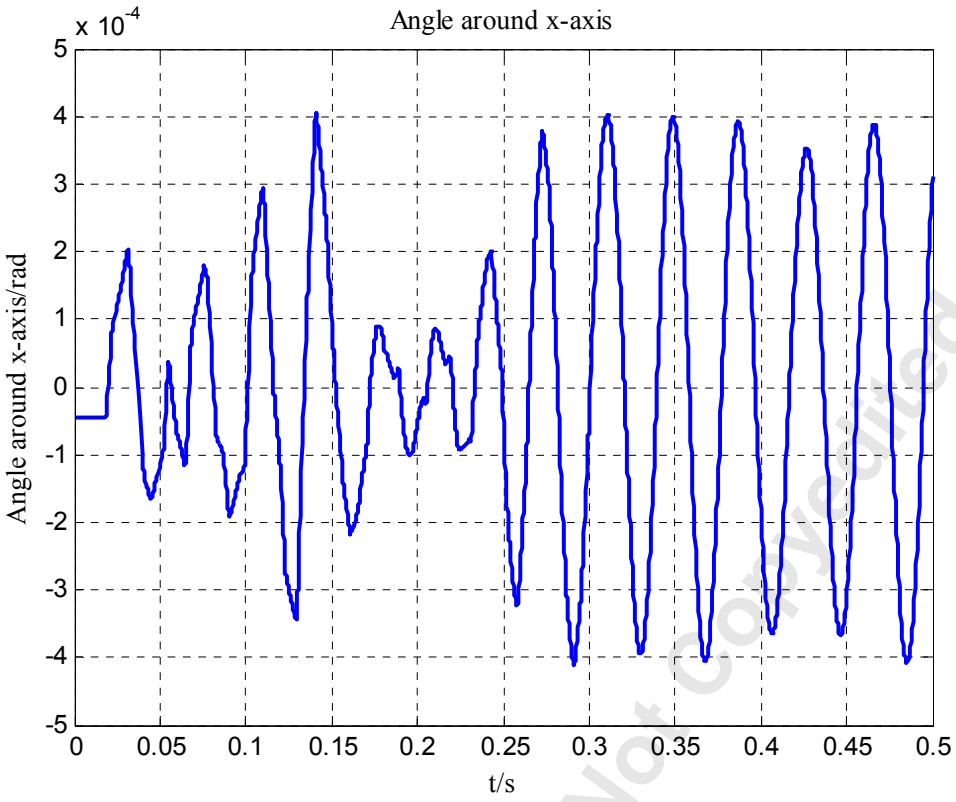

Fig 11. Predicted angle around x-axis, Case I-1

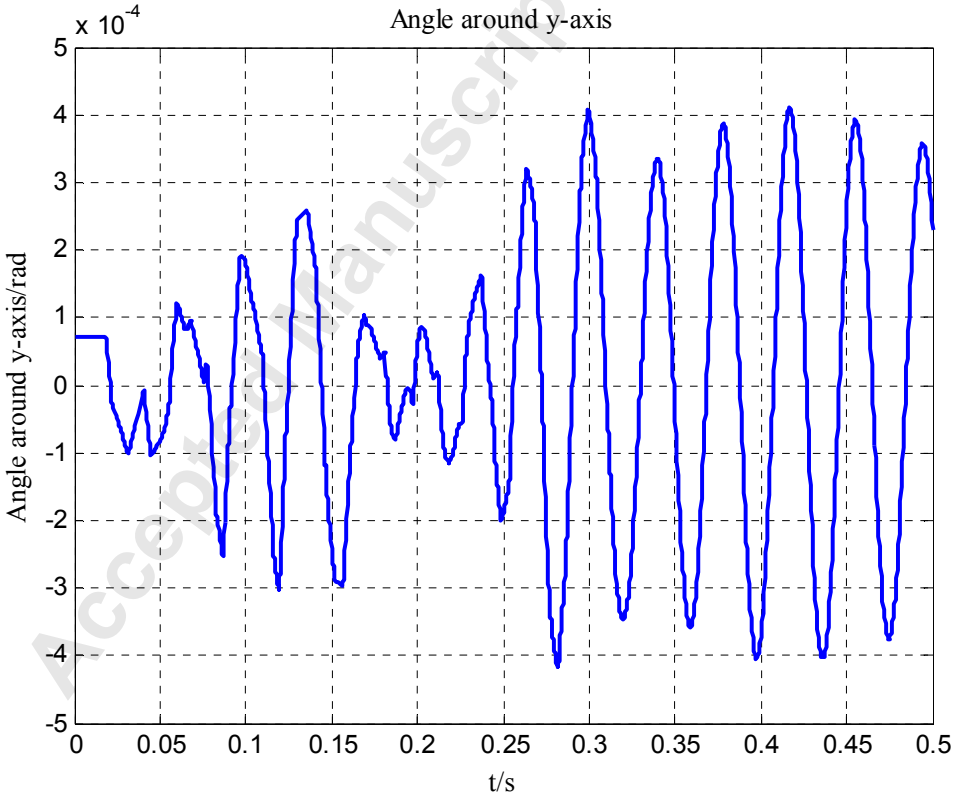

Fig 12. Predicted angle around y-axis, Case I-1

Journal of Tribology. Received April 21, 2016;
Accepted manuscript posted December 1, 2016. doi:10.1115/1.4035343

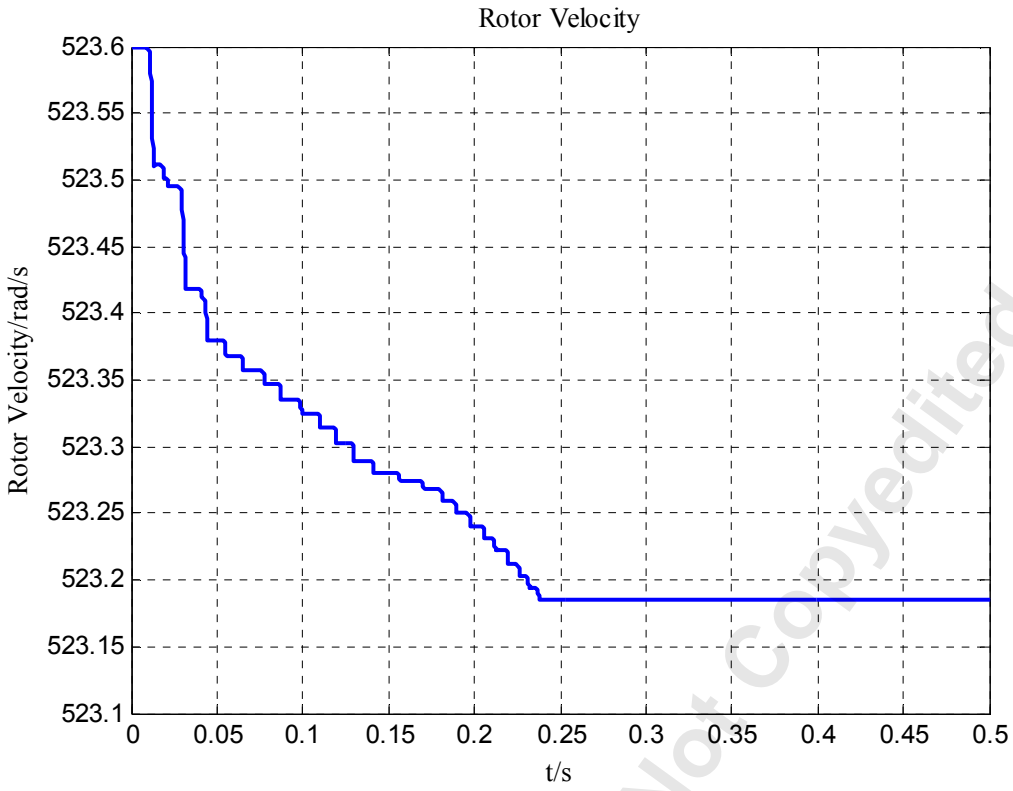

Fig 13. Rotor velocity, Case I-1

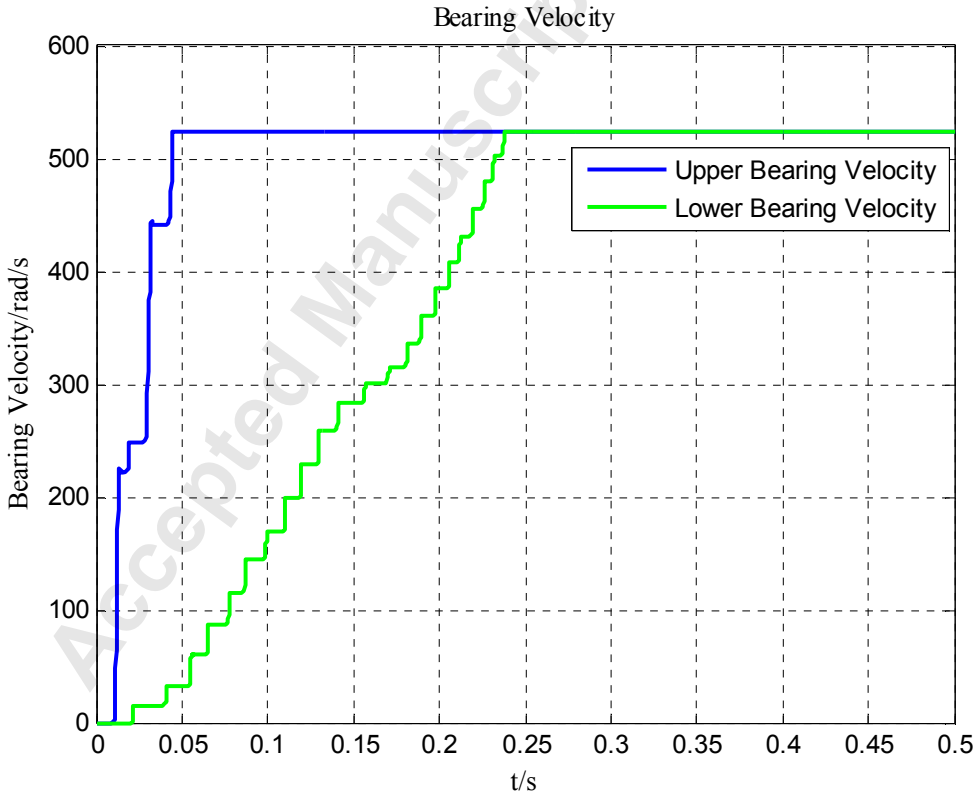

Fig 14. Bearing velocity, Case I-1

Journal of Tribology. Received April 21, 2016;
Accepted manuscript posted December 1, 2016. doi:10.1115/1.4035343

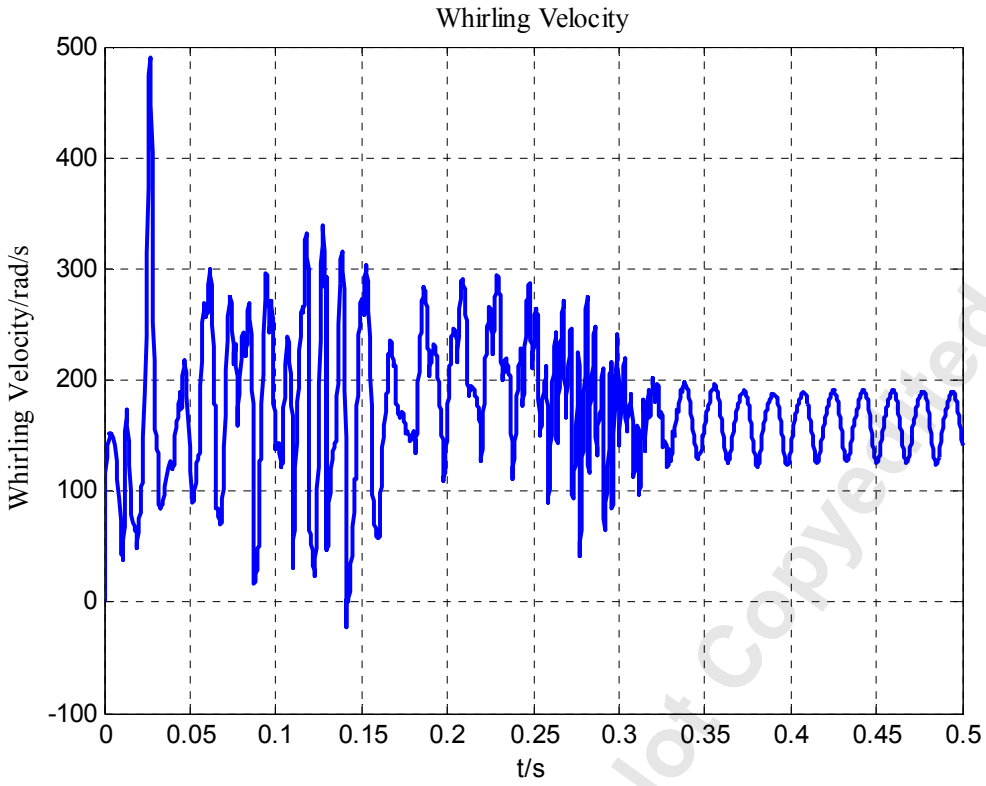

Fig 15. Whirling velocity, Case I-1

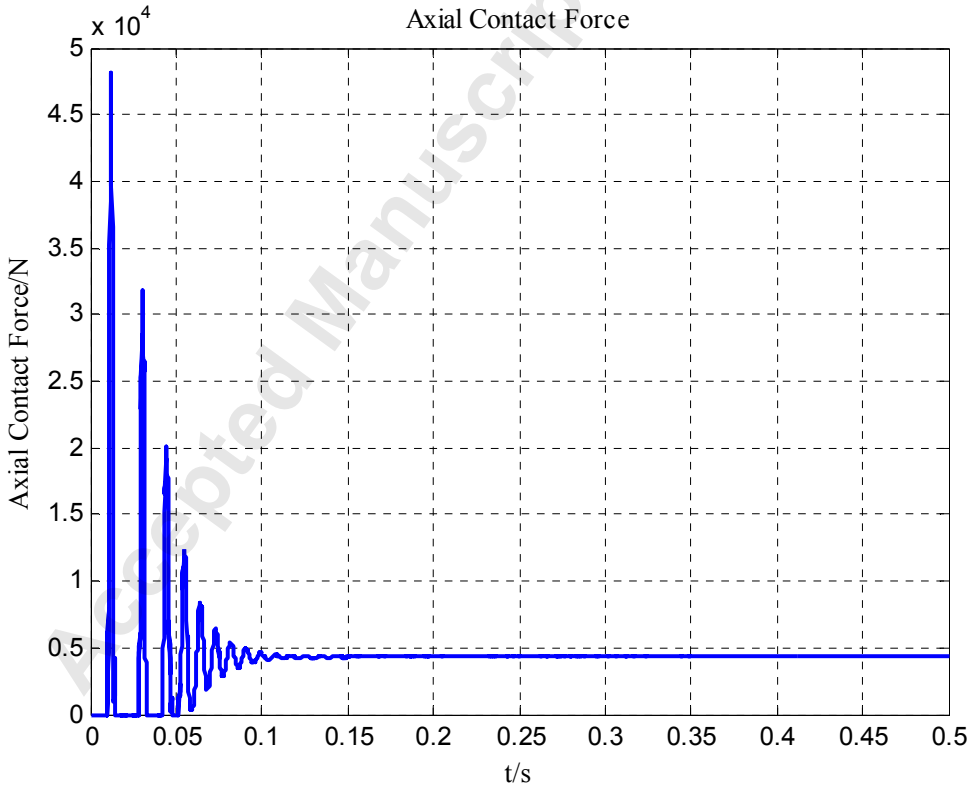

Fig 16. Axial contact force, Case I-1

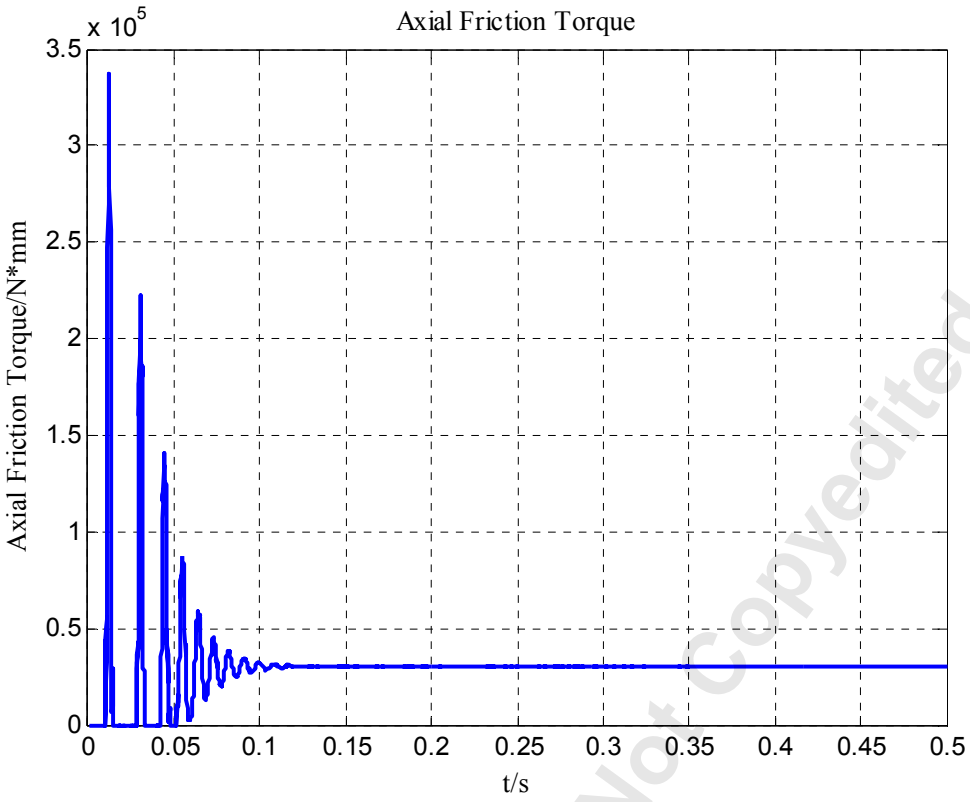

Fig 17. Axial friction torque, Case I-1

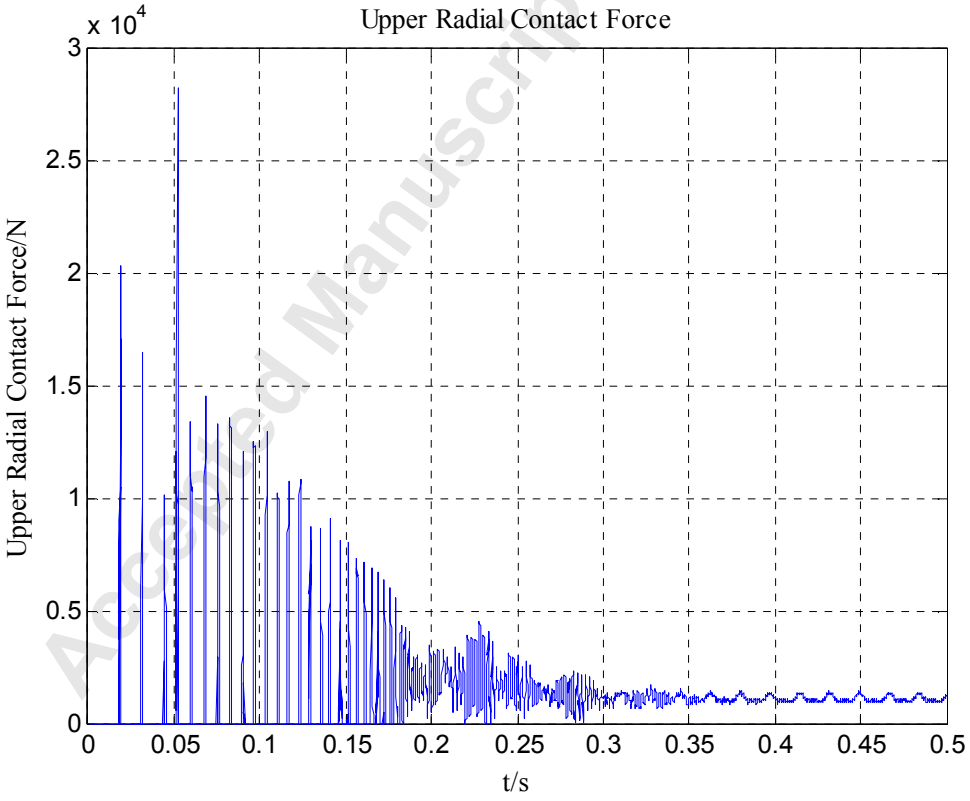

Fig 18. Upper radial contact force, Case I-1

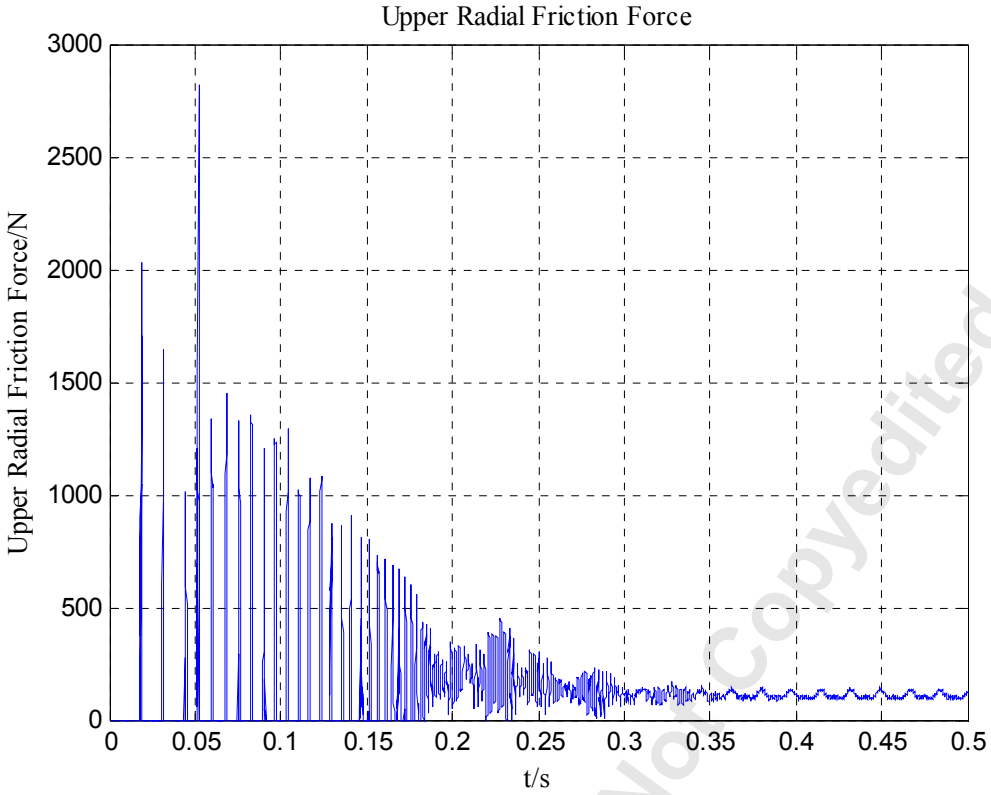

Fig 19. Upper radial friction force, Case I-1

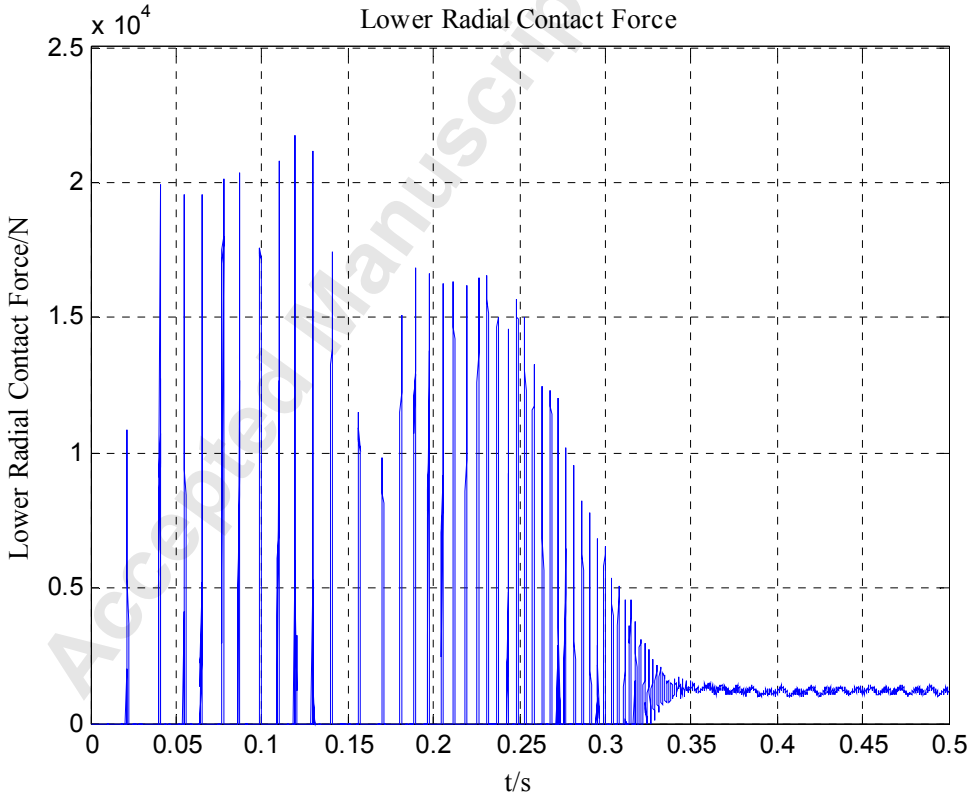

Fig 20. Lower radial contact force, Case I-1

Journal of Tribology. Received April 21, 2016;
Accepted manuscript posted December 1, 2016. doi:10.1115/1.4035343

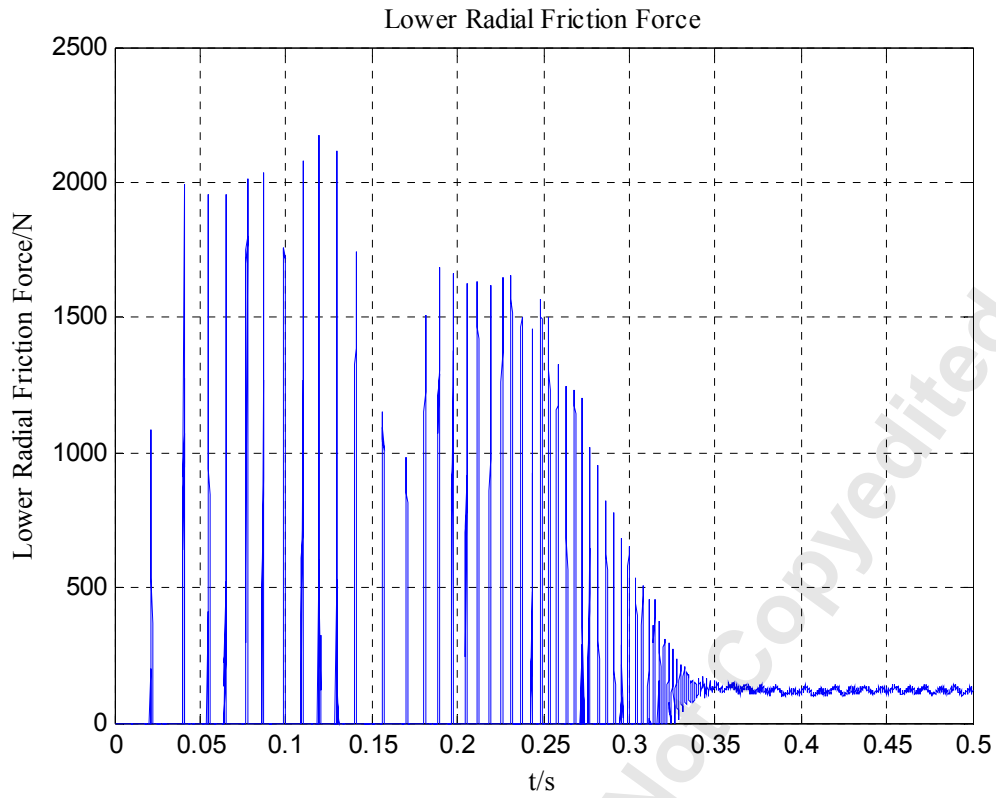

Fig 21. Lower radial friction force, Case I-1

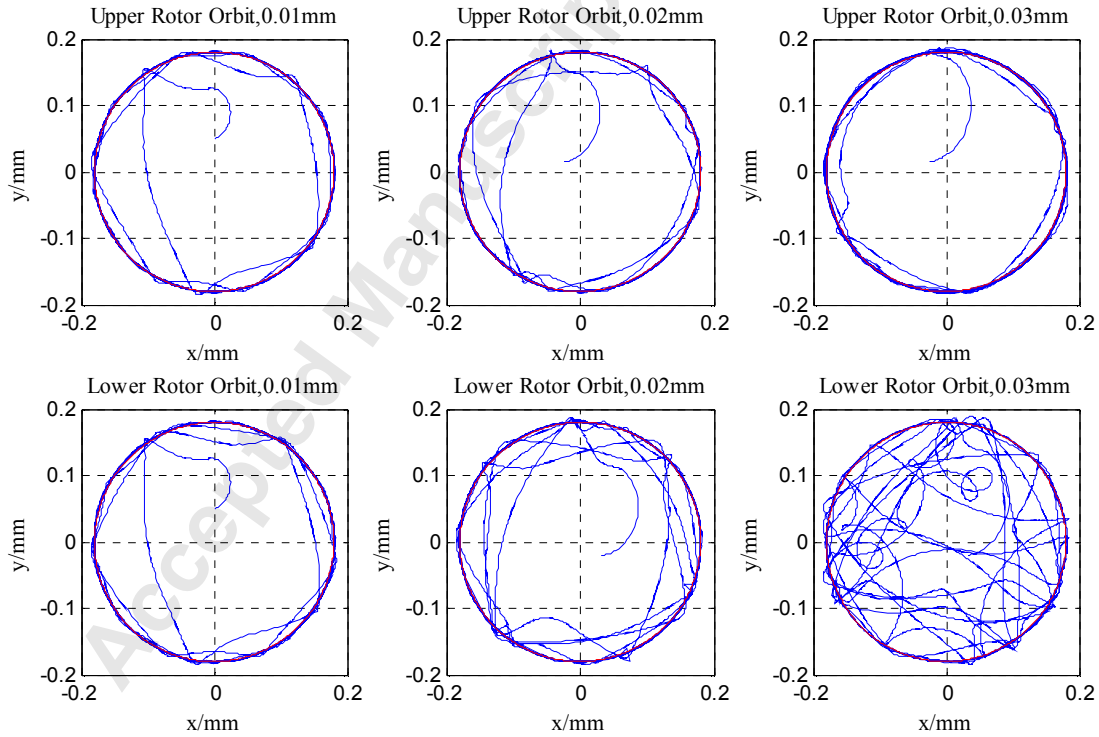

Fig 22. Predicted rotor orbits

3.2 Friction coefficient

Cases II-1 to 3 were conducted to evaluate the effect of the axial friction coefficient, which is an important factor to assess in the rotor drop process. The influences to the drop down procedure are discussed in the following analysis. The comparison of the predicted rotor orbits is listed in Fig.23. The initial condition of these cases is assumed that the upper and lower orbits have a similar initial position. Therefore in these cases the initial condition is attributed to the cylindrical motion. The orbits of these two cross sections have a similar trend in the same orientation. The rotor drop process is rather sensitive to the initial condition.

Figure 24 is obtained from the comparison of whirling velocity among these cases. There is a positive correlation between the steady whirling velocity and the friction coefficient. Thus a solution to reduce the forward whirl motion is to alleviate the friction coefficient while under some circumstances reducing the friction coefficient may affect the simulation stability. This is purely numerical in the simulation and caused by numerical sensitivity to reduced system damping from lower friction forces. Another aspect that friction coefficient affects is the contact force illustrated in Fig.25. It is noted that the influence to the peak axial contact force is rather limited. Peak axial contact force doesn't vary significantly when the friction coefficient changing. Nevertheless the peak radial contact forces of the upper and lower bearings vary with the friction coefficient. The friction coefficient clearly affects the radial contact.

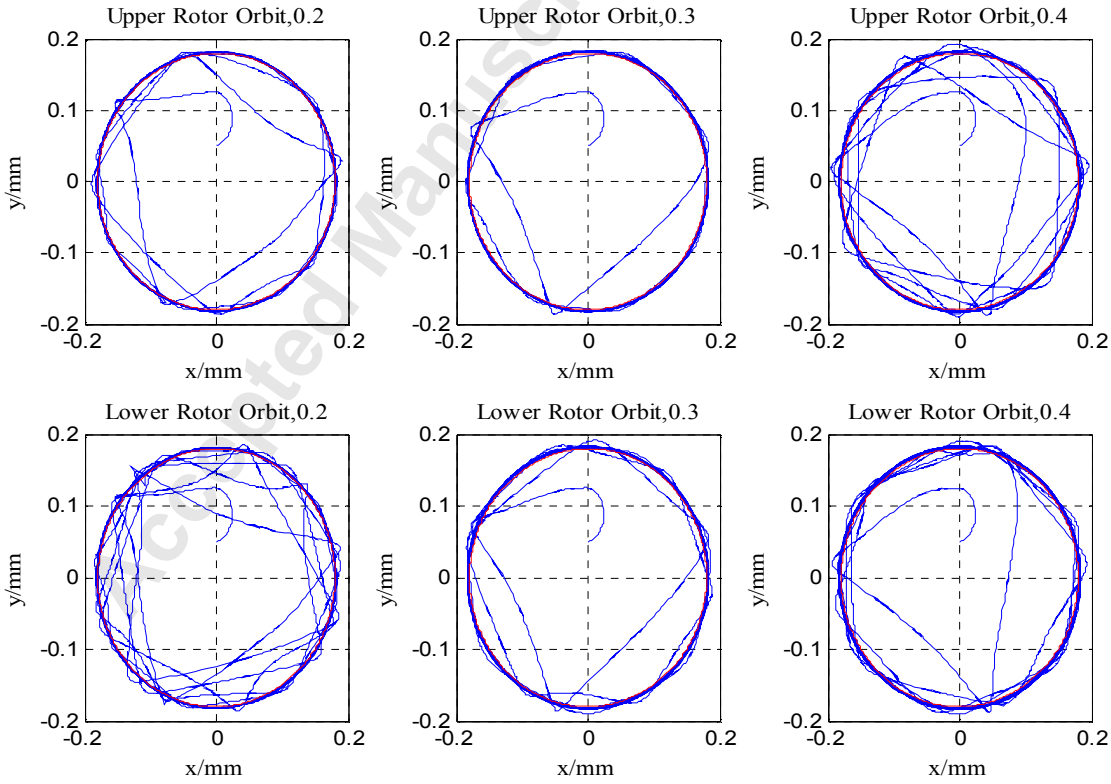

Fig 23. Predicted rotor orbit

Journal of Tribology. Received April 21, 2016;
Accepted manuscript posted December 1, 2016. doi:10.1115/1.4035343

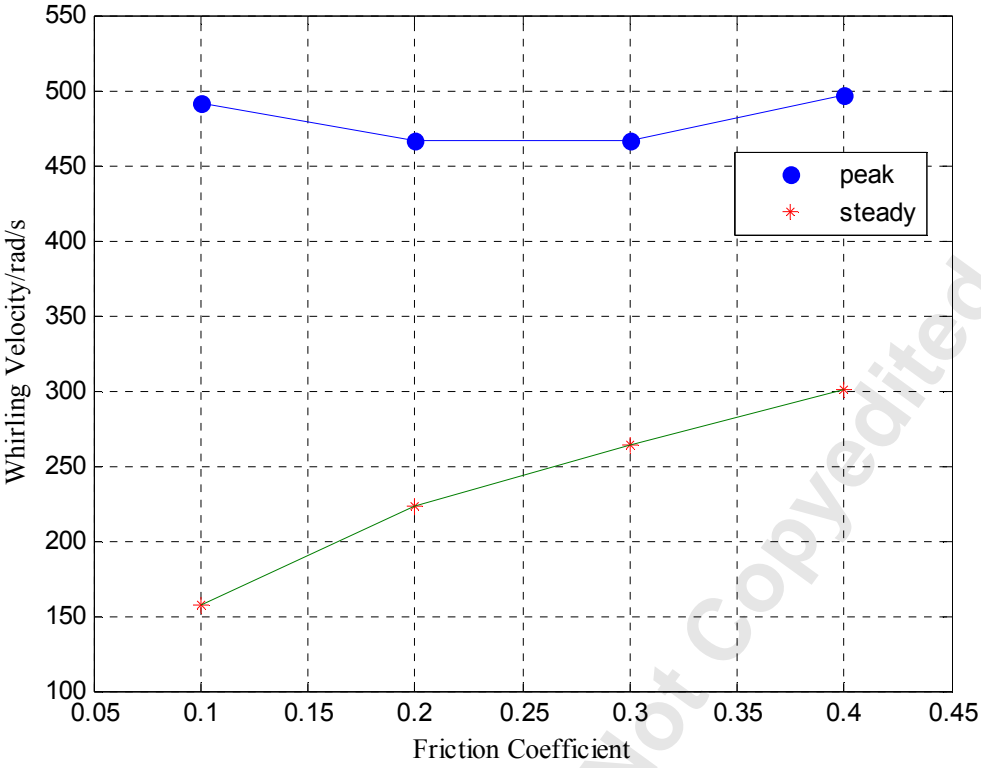

Fig 24. Predicted whirling velocity

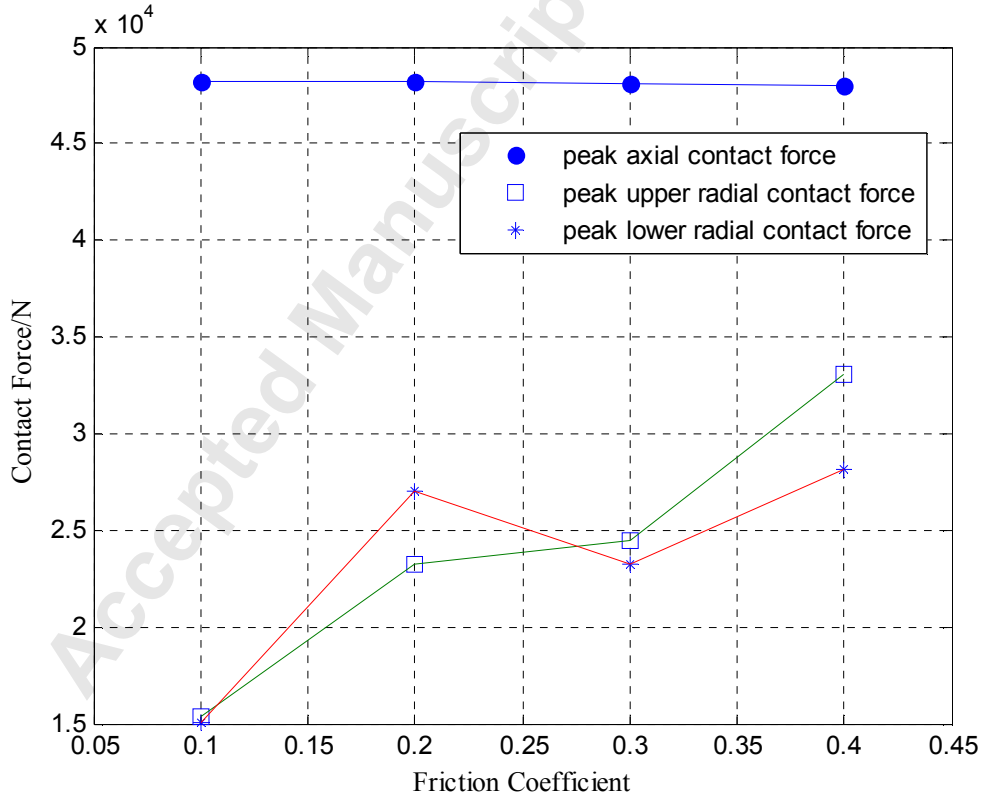

Fig 25. Contact force

3.3 Initial velocity

The rotor motion influenced by the initial velocity is discussed in the following analysis. The difference of the rotor orbits (Cases III-1 and 2) is shown in Fig.26. It's observed from the simulation that tendency to full whirl decreases as the initial velocity decreasing. Additionally, the experimental result shown in Fig.27 also manifests this tendency. The rotor drops with different initial rotational frequencies, 20 Hz, 40 Hz and 60 Hz, respectively.

When the velocity is slow enough, the contact motion is greatly reduced. The experimental results also show that the whiling motion especially in the lower orbit isn't developed as fully as the model predicts. Moreover, as shown in Fig.28, the peak whirling velocity increase monotonically with the increase of velocity while the steady whirling velocity remains almost the same. The comparison results for contact forces are revealed in Fig.29. The peak radial contact forces grow with the increase of velocity while the axial contact force remains almost the same. The key aspect of this analysis is that we can alleviate whirling motion by reducing the initial velocity of the rotor. Lower velocity with which the rotor drops will reduce the radial contact. It is also indicated that when the initial velocity is above 3500 rpm, the contact force of the upper auxiliary bearing is much higher. When the initial velocity is below 3500 rpm, the contact force of the lower auxiliary bearing is higher.

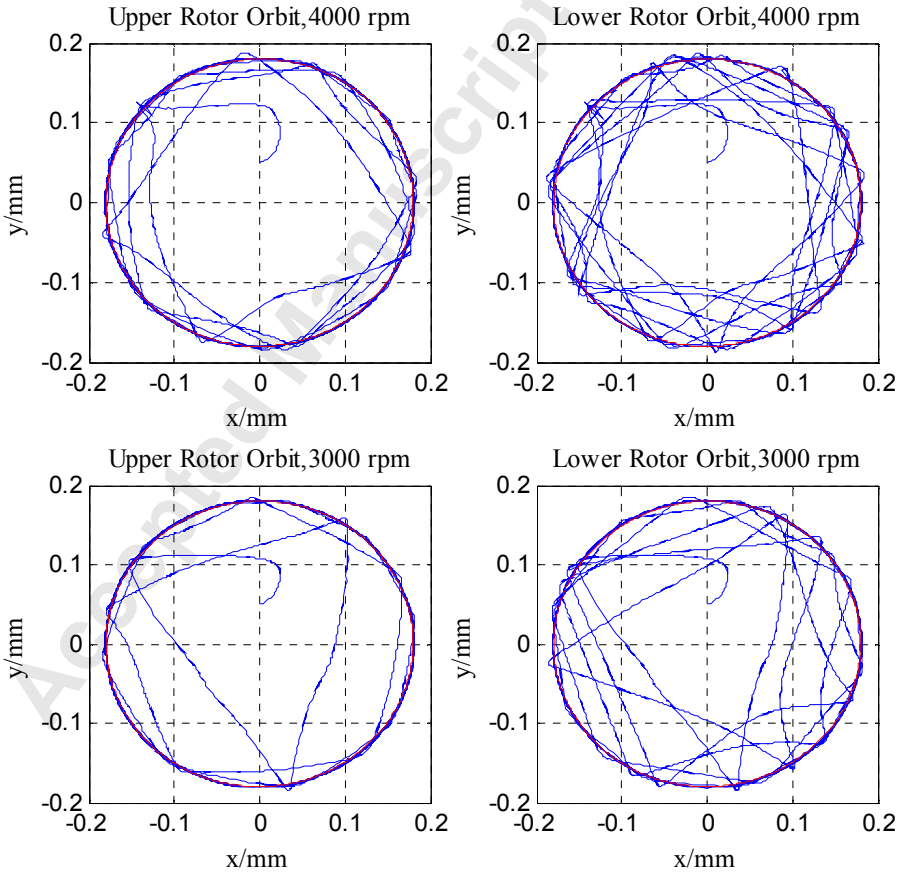

Fig 26. Predicted rotor orbit

Journal of Tribology. Received April 21, 2016;
Accepted manuscript posted December 1, 2016. doi:10.1115/1.4035343

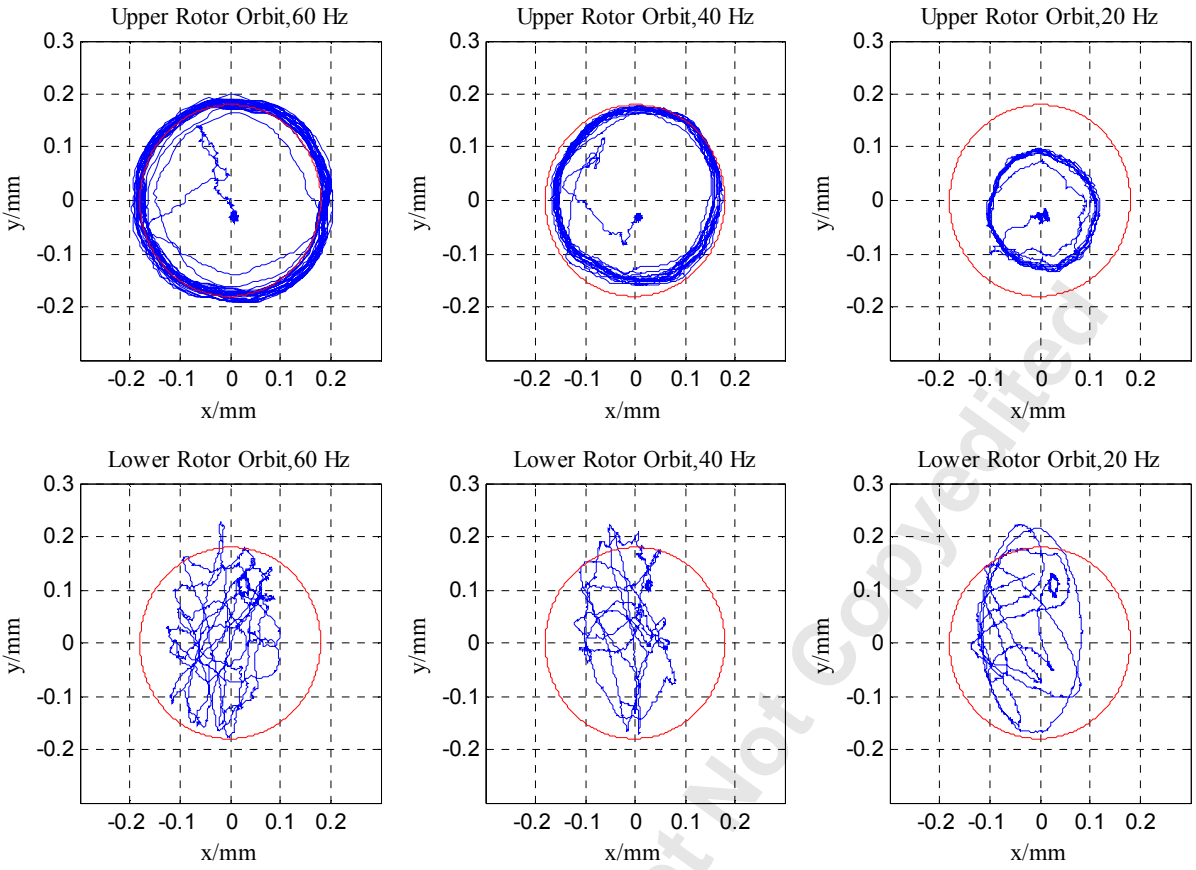

Fig 27. Experimental rotor orbit

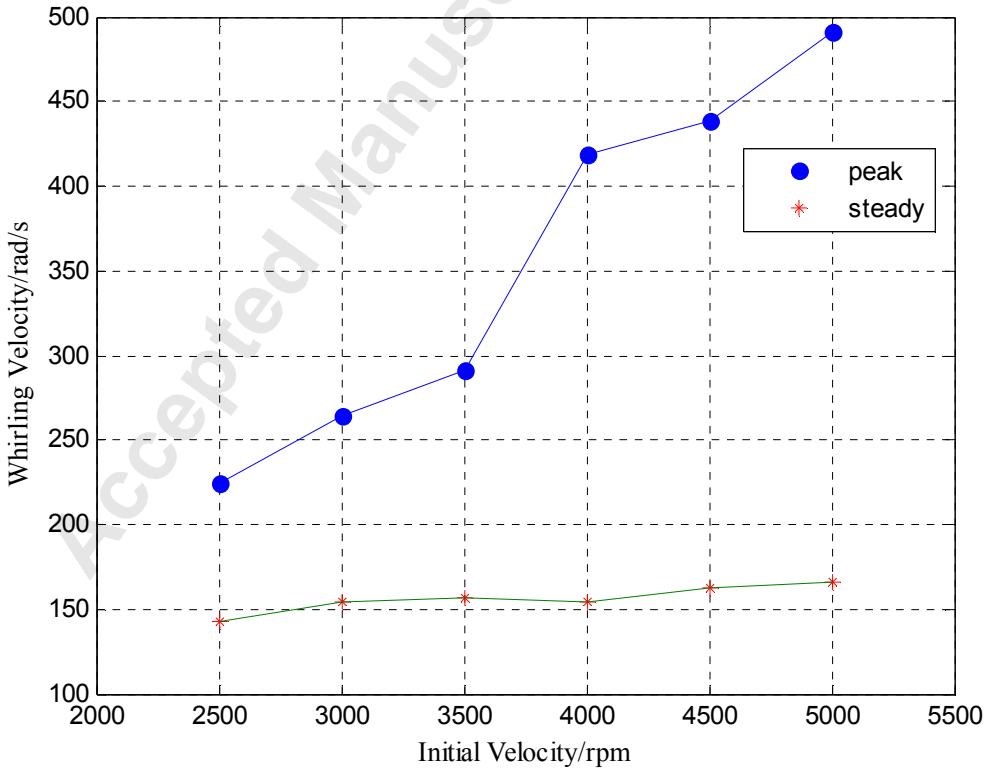

Fig 28. Predicted whirling velocity

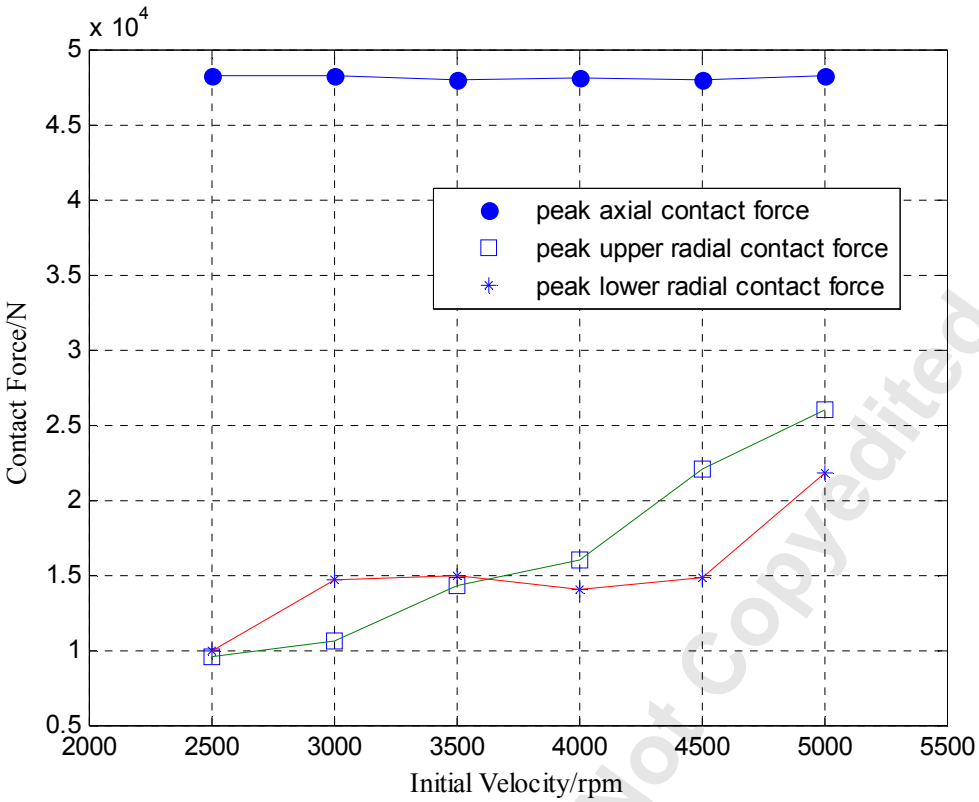

Fig 29. Contact force

3.4 Aerodynamic loading force

The dynamic rotor drop model mainly simulates the process that the rotor drops onto the auxiliary bearing with no aerodynamic force. Nevertheless the blades mounted under the rotor of the helium circulator may induce axial aerodynamic loading force during the rotor drop process. The loading force is approximately 2000 N in the simulation. Case IV is cited as an instance to discuss the influence of aerodynamic loading force. The predicted orbits from a full speed drop with aerodynamic loading force are presented in Fig.30, 31 and 32. Accordingly, the experimental results are plotted in Figs.33, 34 and 35. Compared with the results obtained in Case I-1, which is without consideration of loading force, the tendency to fully developed whirl is much more obvious. The simulation results show consistent trends with the test data although the radial contact happening on the lower bearing is not developed as fully as prediction. The axial and radial contact forces are shown in Figs.36, 37 and 38, respectively. There is no significant difference between the tendencies of the radial contact force, while the peak value of the axial contact force is about 6.13×10^4 N, which is greater than that with no loading force. The axial contact force applied on the inner race is the main force to accelerate the velocity. Given this as shown in Figs.39 and 40 the period to arrive at the same velocity is 0.2 s which is shorter than that of Case I-1, which is 0.25 s.

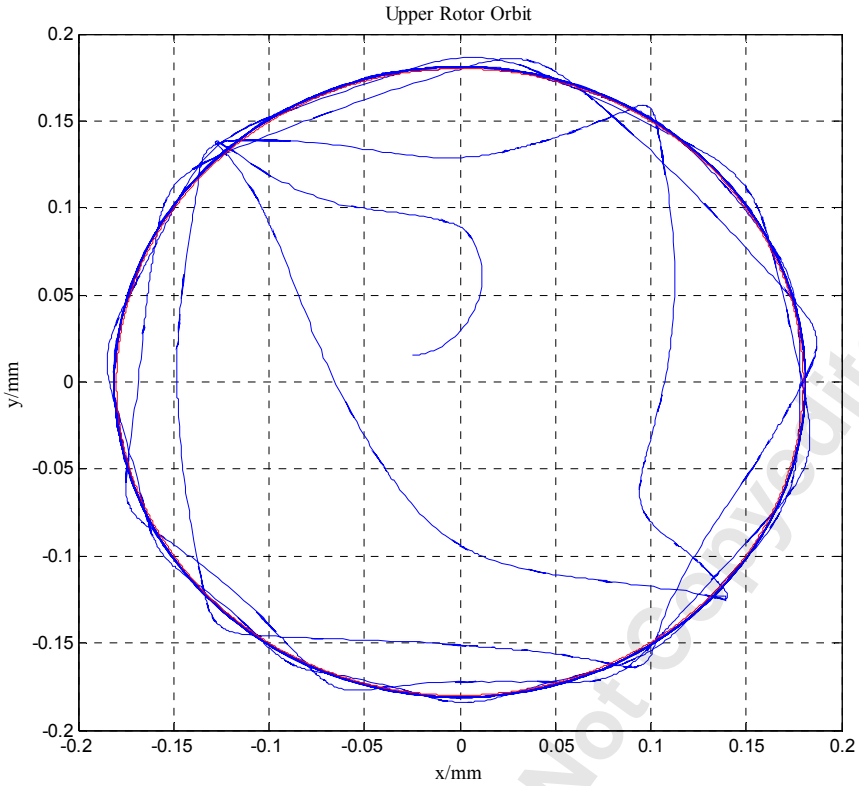

Fig 30. Predicted upper rotor orbit, Case IV

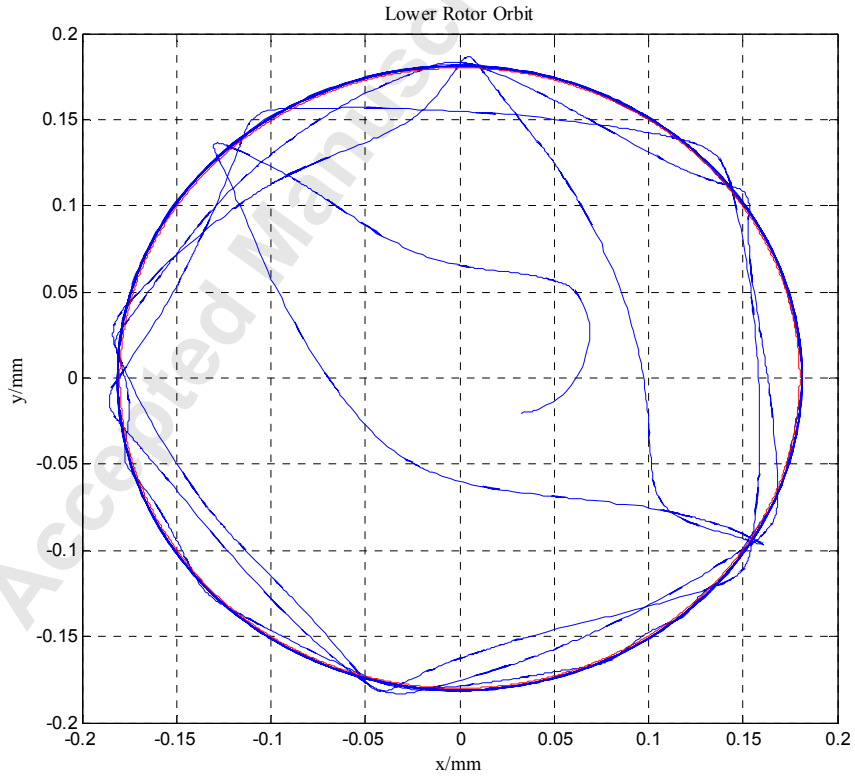

Fig 31. Predicted lower rotor orbit, Case IV

Journal of Tribology. Received April 21, 2016;
Accepted manuscript posted December 1, 2016. doi:10.1115/1.4035343

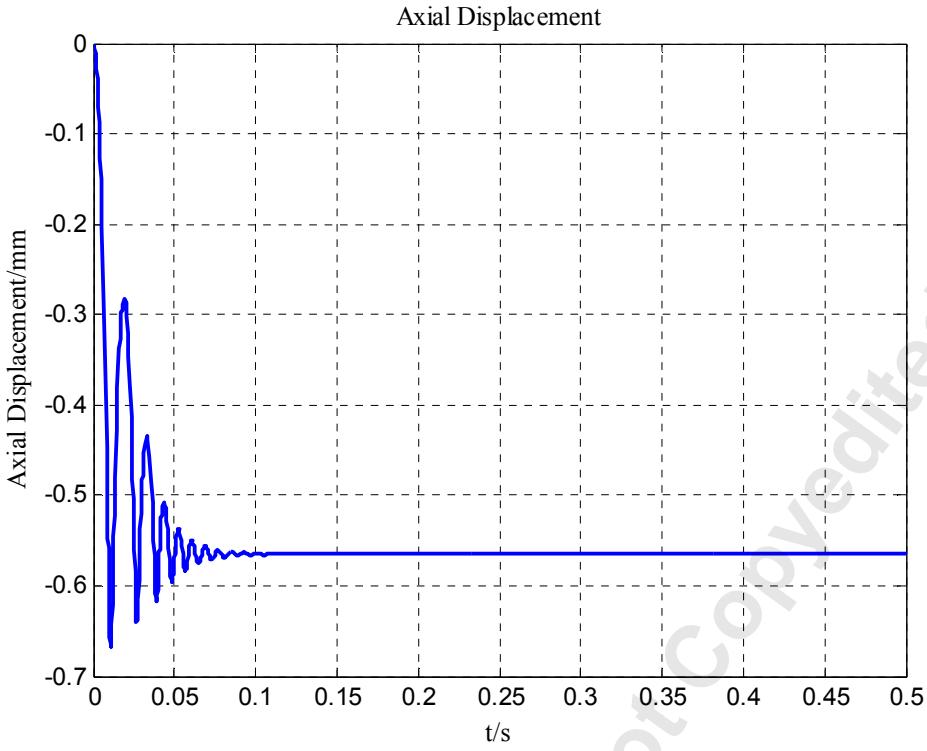

Fig 32. Predicted axial displacement, Case IV

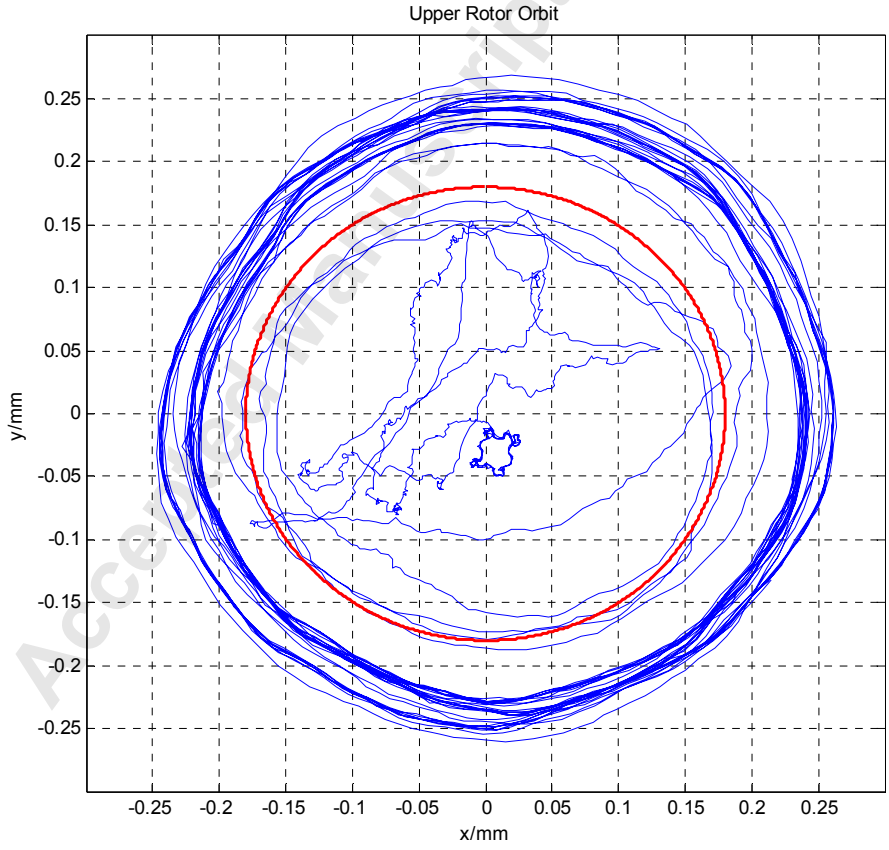

Fig 33. Experimental upper rotor orbit, Case IV

Journal of Tribology. Received April 21, 2016;
Accepted manuscript posted December 1, 2016. doi:10.1115/1.4035343

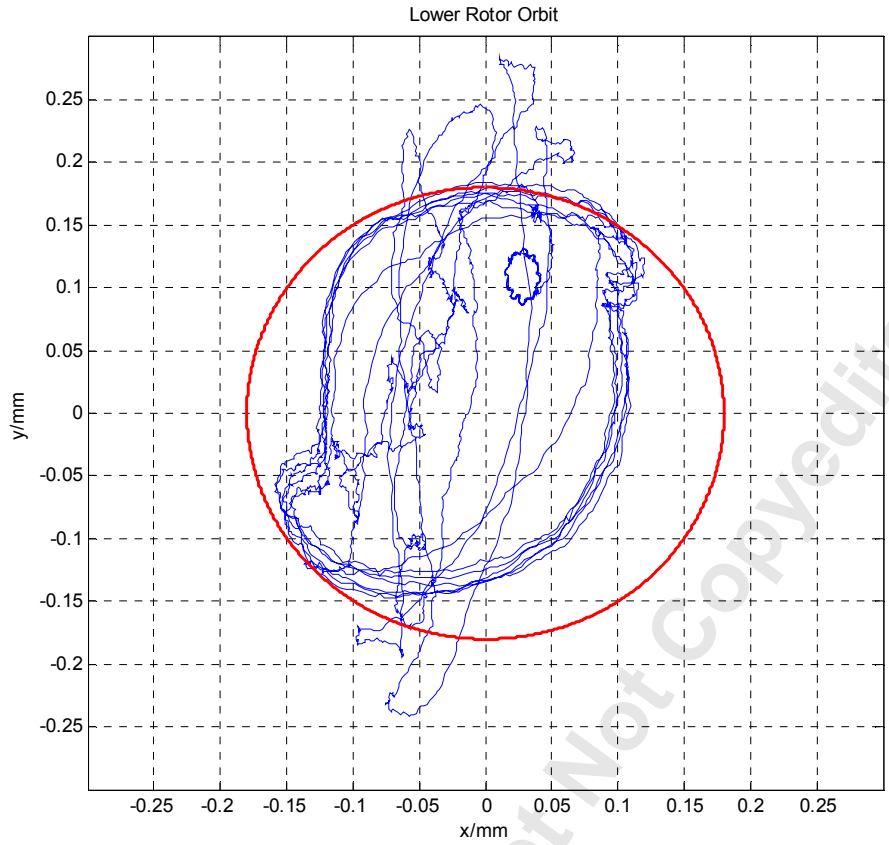

Fig 34. Experimental lower rotor orbit, Case IV

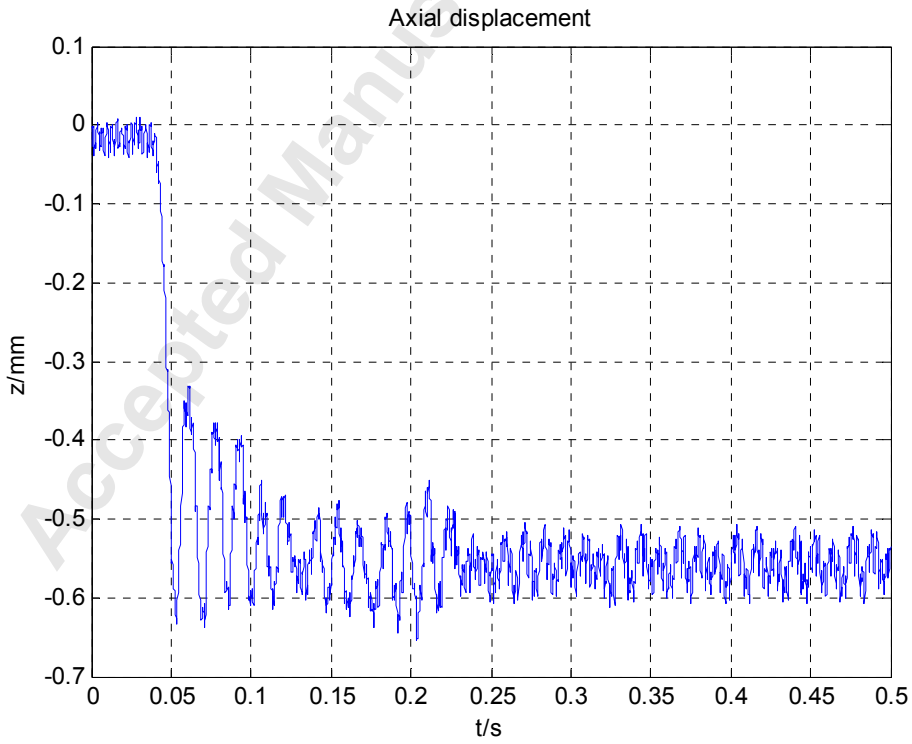

Fig 35. Experimental axial displacement, Case IV

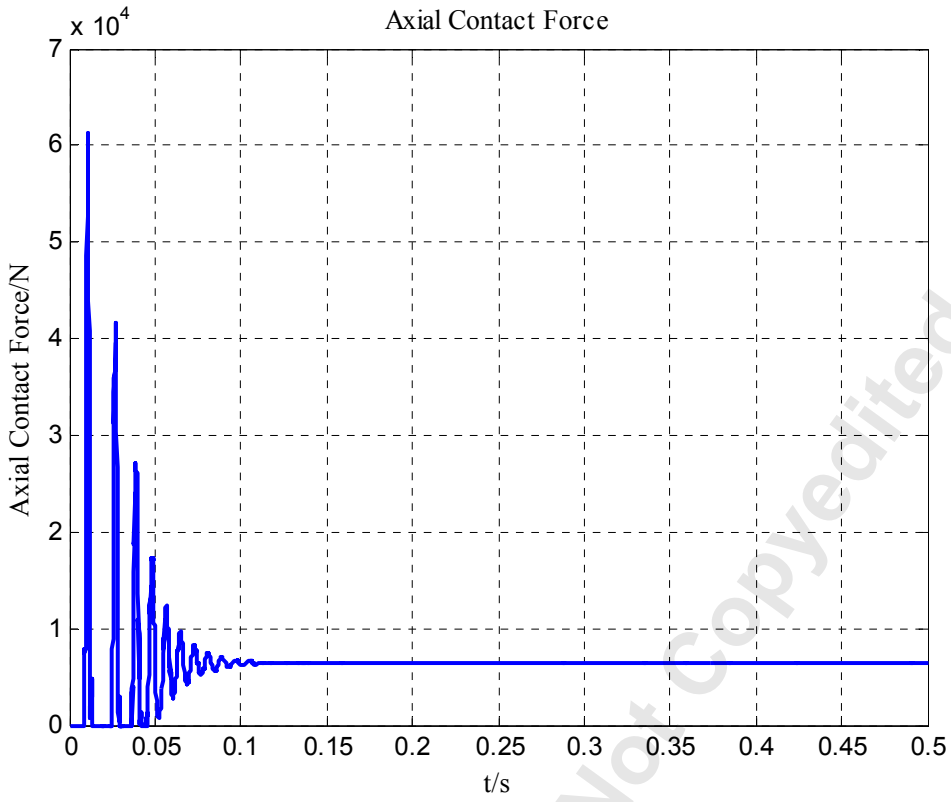

Fig 36. Axial contact force, Case IV

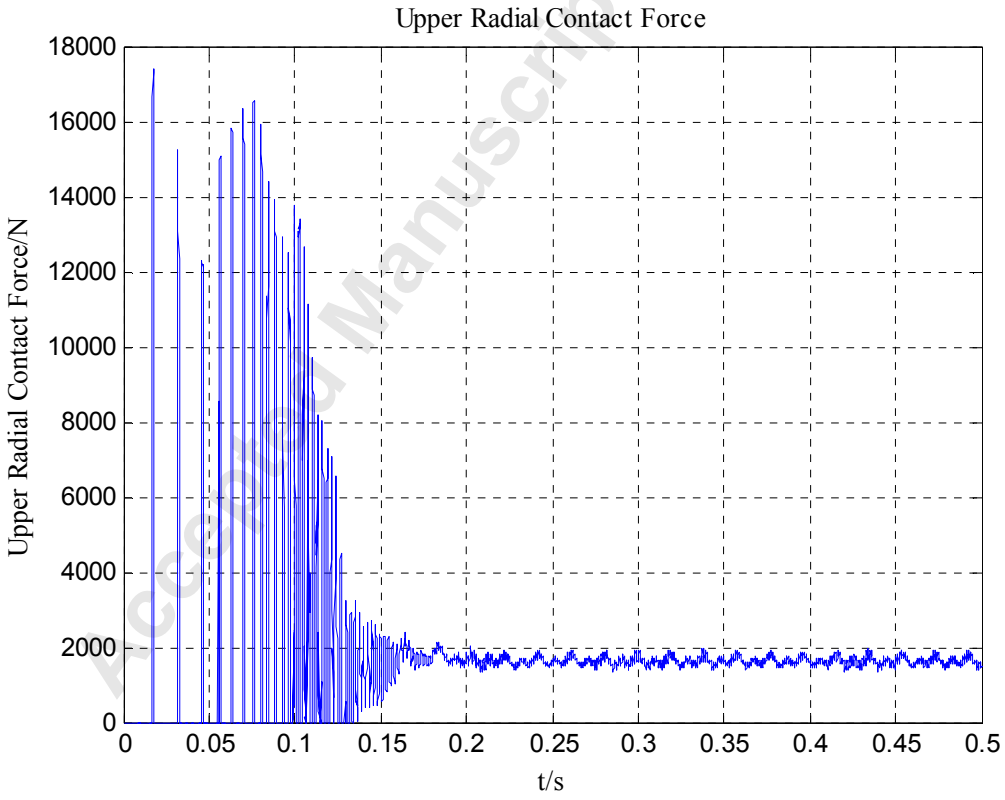

Fig 37. Upper radial contact force, Case IV

Journal of Tribology. Received April 21, 2016;
Accepted manuscript posted December 1, 2016. doi:10.1115/1.4035343

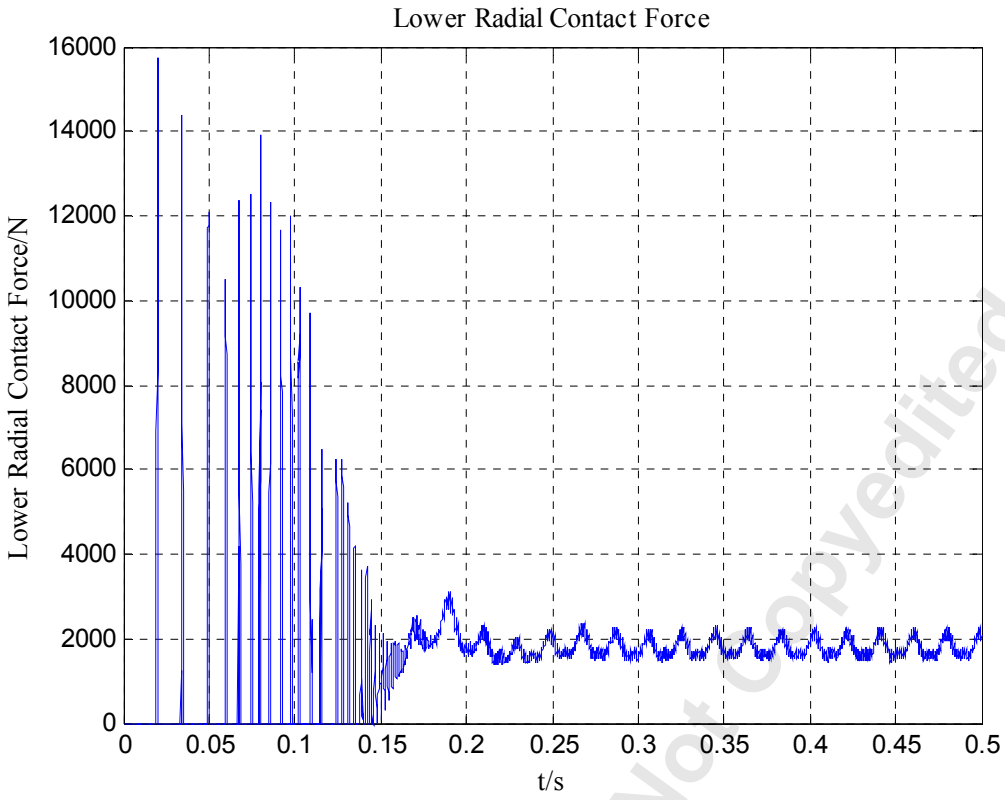

Fig 38. Lower radial contact force, Case IV

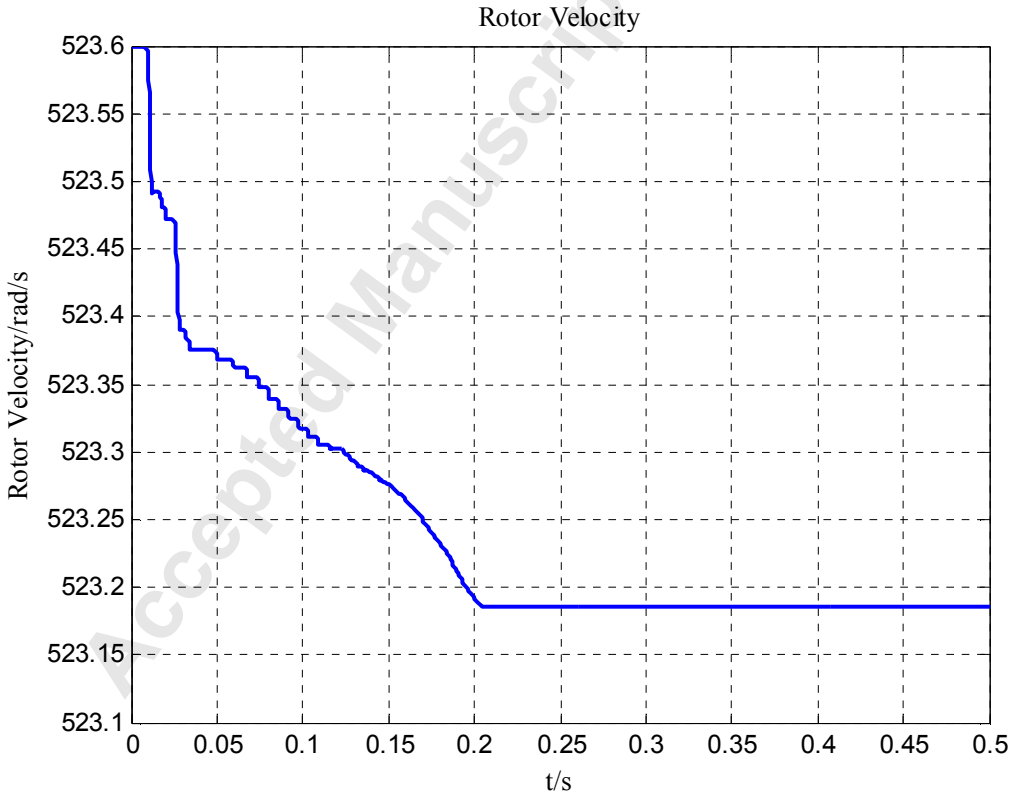

Fig 39. Rotor velocity, Case IV

Journal of Tribology. Received April 21, 2016;
Accepted manuscript posted December 1, 2016. doi:10.1115/1.4035343

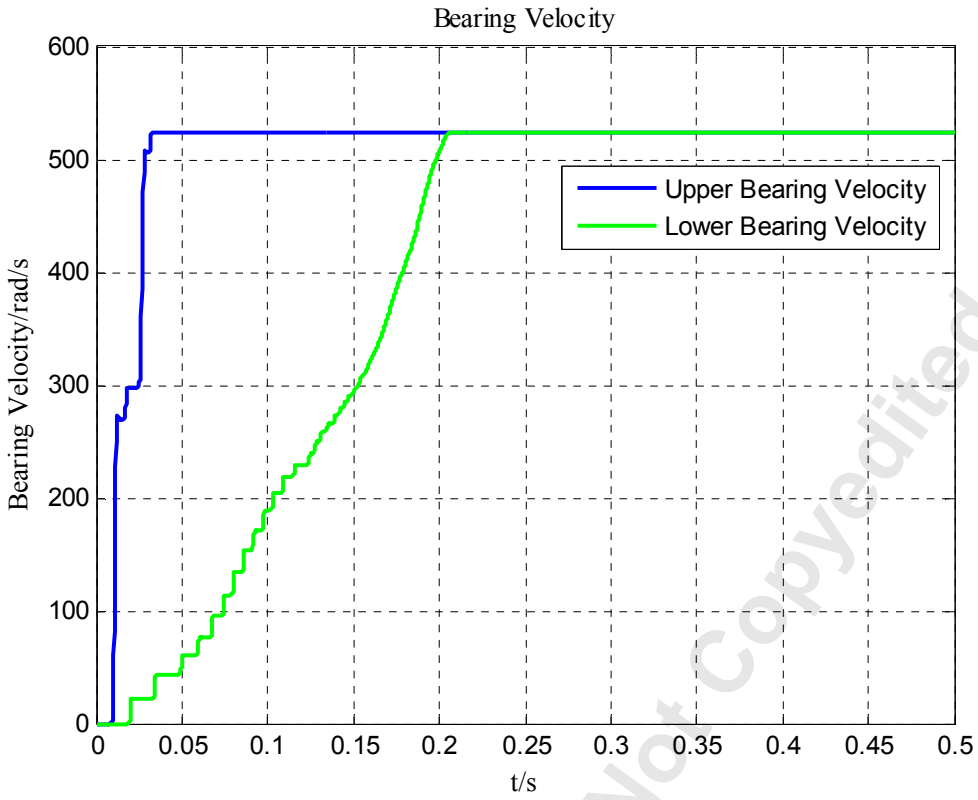

Fig 40. Bearing velocity, Case IV

4. Conclusions

This paper presents a comprehensive analysis of the drop of an AMB levitated vertical rotor onto auxiliary bearings. It considers contact forces and torque that depend on contact condition, including dependence on rolling and sliding friction. The model simulated in this paper adds certain precision than previous models. Also rotor drop simulations are conducted to illustrate the implementation of the auxiliary bearing model. The predicted data show similar trends with the measured data from a realistic test rig. Specifically,

a) The dynamic friction coefficient is a critical parameter that induces forward rotor whirl under contact. The peak axial contact force is, however, only weakly dependent on the friction coefficient. In contrast, the peak radial contact forces increase with the value of the friction coefficient.

b) The initial rotor velocity, which may be of unknown value in operational conditions, is liable to increase the onset of rotor whirl if high. Lower initial rotor velocity alleviates the onset of full whirl.

c) Axial aerodynamic force tends to increase the peak axial contact force, though the time taken for the rotor to enter rolling contact with the auxiliary bearing is reduced.

In conclusion, the results in this paper will contribute to the further improvement of auxiliary bearing design and engineering application.

Acknowledgment

This paper is supported by the National Natural Science Foundation of China (No. 51275261) and National S&T Major Project (No. ZX069).

Nomenclature

a = location of upper auxiliary bearing
b = location of lower auxiliary bearing
C = contact damping
e = contact parameter / rotor imbalance eccentricity
F = contact force
F_t = radial friction force
I_b = moment of inertia of auxiliary bearing
I_p = polar moment of inertia of rotor
K = contact stiffness
m = mass
O_b = geometric center of auxiliary bearing
O_c = mass center of rotor
O_r = geometric center of rotor
P_a = axial contact pressure
q_i = generalized coordinator
Q_i = generalized force
R_{b1} = inner radius of inner race
R_{b2} = outer radius of inner race
R_r = radius of rotor
T = kinetic energy / torque
V = gravitational potential energy
x = displacement in x direction
y = displacement in y direction
z = displacement in z direction
z' = rotating axis
α = angular between O_bO_r and x -axis
γ = rotating angular of rotor
δ = impact depth
$\dot{\theta}$ = precession angular velocity of rotor in y-axis
$\dot{\theta}_b$ = velocity of auxiliary bearing
μ = friction coefficient
ρ = relative distance between O_b and O_r
$\dot{\varphi}$ = precession angular velocity of rotor in x-axis

Subscripts

a = axial
b = bearing
f = friction
i = i axis
j = j axis
r = radial
x = x axis
y = y axis
1 = upper auxiliary bearing
2 = lower auxiliary bearing

References

[1] Schweitzer, G., 1994, Active Magnetic Bearings, Vdf Hochschulverlag AG an der ETH Zurich, Zurich Switzerland.

[2] Yang, G., Shi, Z., Zhao, J., and Yu, S., 2013, "Reliability Analysis of Helium Blower Auxiliary Bearings for HTR-10," SMiRT-22, San Francisco, CA, August 18–23.

[3] Kärkkäinen, A., Sopanen, J., and Mikkola, A., 2006, "Simulation of AMB supported rotor during drop on Retainer bearings," Research report, Lappeenrannan teknillinen yliopisto, Konetekniikan osasto.

[4] Sun, G., Palazzolo, A. B., Provenza, A., and Montague, G., 2004, "Detailed Ball Bearing Model for Magnetic Suspension

Auxiliary Service," Journal of Sound and Vibration, 269(3–5), pp. 933–963.

[5] Sun, G., 2006, "Rotor Drop and Following Thermal Growth Simulations Using Detailed Auxiliary Bearing and Damper Models," Journal of Sound and Vibration, 289(1–2), pp. 334–359.

[6] Lee, J. G., and Palazzolo, A. B., 2012, "Catcher Bearing Life Prediction Using a Rainflow Counting Approach," Journal of Tribology, 134(3), p. 031101.

[7] Keogh, P. S., and Yong, W. Y., 2007, "Thermal Assessment of Dynamic Rotor/Auxiliary Bearing Contact Events," Journal of Tribology, 129(1), pp. 143–152.

[8] Schlotter, M., and Keogh, P. S., 2007, "Synchronous Position Recovery Control for Flexible Rotors in Contact with Auxiliary Bearings," Journal of Vibration and Acoustics, 129, pp. 550-558.

[9] Caprio, M., Murphy, B., and Herbst, J., 2006, "Spin commissioning and drop tests of a 130 kW-hr composite flywheel," The Ninth International Symposium on Magnetic Bearing, KY, USA, August.

[10] Hawkins, L., McMullen, P., and Larsonneur, R., 2005, "Development of an AMB Energy Storage Flywheel for Commercial Application," 8th International Symposium on Magnetic Suspension Technology (ISMST-8), Dresden, Germany, Sept.

[11] McMullen, P., Vuong, V., and Hawkins, L.,2006, "Flywheel energy storage system with AMB's and hybrid backup bearings," 10th International Symposium on Magnetic Bearings, Martigny, Switzerland.

[12] Ransom, D., Masala, A., Moore, J., Vannini, G., Camatti, G., and Lacour, M., 2009, "Development and Application of a Vertical High Speed Motor-Compressor Simulator for Rotor Drop onto Auxiliary Bearings," Proceedings of the 38th Turbomachinery Symposium, Houston, TX, September.

[13] Wilkes, J., Moore, J., Ransom, D., and Vannini, G., 2013, "An Improved Catcher Bearing Model and an Explanation of the Forward Whirl/Whip Phenomenon Observed in Active Magnetic Bearing Transient Drop Experiments," ASME Turbo Expo 2013: Turbine Technical Conference and Exposition, San Antonio, Texas, USA, June 3–7.

[14] Xu, Y., and Zuo, K., "Overview of the 10 MW high temperature gas cooled reactor-test module project," Nuclear Engineering and Design, 218, pp. 13-23.

[15] Zhao, J., Yang, G., Li, Y., and Yu, S., 2012, "Numerical Analysis of Magnetically Suspended Rotor in HTR-10 Helium Circulator Being Dropped into Auxiliary Bearings," Nuclear Power Engineering, 33, pp. 61-64.

[16] Xiao, Z., Yang, G., Li, Y., Shi, Z., and Yu, S., 2014, "Performance Assessment of Auxiliary Bearing in HTR-10 AMB Helium Circulator on the Event of Rotor Drop," Nuclear Power Engineering, 35, pp. 82-85.

[17] Kang, X., Yang, G., and Yu, S., 2014, "Dynamic Behavior of the AMB's Vertical Arranged Rotor During its Drop Process," Proceedings of the 22th International Conference on Nuclear Engineering, Prague, Czech, July.

[18] Zhao, Y., Yang, G., Shi, Z., and Zhao, L., 2015, "Thermal Analysis and Simulation of Auxiliary Bearings and Its Application in the High Temperature Reactor-10," Journal of Tribology, 138 (1), pp. 1-11.

[19] Palmgren, 1959, Ball and Roller Bearing Engineering, 3rd Ed, Burbank, Philadelphia.